UNIVERSITY *of York*

This is a repository copy of *The primary familial brain calcification associated protein MYORG is an α-galactosidase with restricted substrate specificity*.

White Rose Research Online URL for this paper:
https://eprints.whiterose.ac.uk/id/eprint/191287/

Version: Accepted Version

Article:

Meek, Richard W., Brockerman, Jacob, Fordwour, Osei B. et al. (3 more authors) (2022) The primary familial brain calcification associated protein MYORG is an α-galactosidase with restricted substrate specificity. PLoS Biol. ISSN: 1544-9173

https://doi.org/10.1371/journal.pbio.3001764

White Rose
university consortium
Universities of Leeds, Sheffield & York

eprints@whiterose.ac.uk
https://eprints.whiterose.ac.uk/

The primary familial brain calcification (PFBC)-associated protein MYORG is an α-galactosidase with restricted substrate specificity.

Richard W. Meek,[a] Jacob Brockerman,[b,c] Osei B. Fordwour,[d] Wesley F. Zandberg,[d,e] Gideon J. Davies,[a,*] David J. Vocadlo[b,c,*,†]

[a] Department of Chemistry. University of York, York, YO10 5DD, United Kingdom.
[b] Department of Molecular Biology and Biochemistry, Simon Fraser University, V5A 1S6, Burnaby, British Columbia, Canada.
[c] Department of Chemistry, Simon Fraser University, Burnaby, V5A 1S6, British Columbia, Canada.
[d] Department of Chemistry, Irving K. Barber Faculty of Science, University of British Columbia, 3247 University Way, , V1V 1V7, Kelowna, British Columbia, Canada.
[e] Department of Biochemistry and Molecular Biology, University of British Columbia, V6T 1Z4, Vancouver, British Columbia, Canada.
*Corresponding Authors: Gideon J Davies and David J. Vocadlo
Email: gideon.davies@york.ac.uk
Email: dvocadlo@sfu.ca
[†]Lead Contact: David J Vocadlo

Final Character count: 61289 (including spaces)

Abstract

Primary familial brain calcification is characterised by abnormal deposits of calcium phosphate within various regions of the brain that are associated with severe cognitive impairments, psychiatric conditions, and movement disorders. Recent studies in diverse populations have shown a link between mutations in myogenesis-regulating glycosidase (MYORG) and the development of this disease. MYORG is a member of glycoside hydrolase (GH) family 31 (GH31) and, like the other mammalian GH31 enzyme α-glucosidase II, this enzyme is found in the lumen of the endoplasmic reticulum. Though presumed to act as an α-glucosidase due to its localization and sequence relatedness to α-glucosidase II, MYORG has never been shown to exhibit catalytic activity. Here we show that MYORG is an α-galactosidase and present the high-resolution crystal structure of MYORG in complex with substrate and inhibitor. Using these structures, we map detrimental mutations that are associated with MYORG-associated brain calcification and define how these mutations may drive disease progression through loss of enzymatic activity. Finally. we also detail the thermal stabilization of MYORG afforded by a clinically approved small molecule ligand, opening the possibility of using pharmacological chaperones to enhance the activity of mutant forms of MYORG.

Introduction

Primary familial brain calcification (PFBC), commonly referred to as Fahr's syndrome, is a set of rare genetic disorders associated with abnormal bilateral deposits of calcium phosphate within various regions of the brain(1). Significant calcification is associated with cognitive impairments, psychiatric conditions, and movement disorders(1). PFBC was generally considered an autosomal dominant disorder caused by genetic abnormalities in just four genes: *SLC20A2*, *XPR1, PDGFRB*, and *PDGFB*(2-5). Recent studies, however, have linked development of PFBC to biallelic loss-of-function mutations in the genes *JAM2* and *MYORG* (**Table S1**)(6, 7). While the function of proteins encoded by *SLC20A2*, *XPR1, PDGFRB*, *PDGFB,* and *JAM2* have previously been described, and have offered some insights into their roles in PFBC progression(8-10), the function and activity of the myogenesis-regulating glycosidase (MYORG) encoded by *MYORG* remain unknown. Given that no treatment options are available for patients with PFBC, there is a need to understand the function of these proteins with the goal of understanding the root causes of PFBC.

We were intrigued by MYORG, which is a type II transmembrane protein predicted to be comprised of a short, disordered nucleocytoplasmic N-terminal region, a single transmembrane helix, and a lumenal C-terminal catalytic region comprising a CAZy family glycoside hydrolase 31 (GH31) catalytic domain and two β-sheet domains (**Figure 1**)(11-13). This GH31 domain has, for a glycan degrading enzyme, a distinctive localization within the early secretory pathway where most glycans typically start to be assembled. Within brain, MYORG is expressed in astrocytes, and in various cell lines it has been shown to be distributed to the endoplasmic reticulum (ER) and nuclear envelope,(6, 11, 14). The lumenal orientation for the GH31 domain of MYORG has been demonstrated using protease digestion experiments(11). This localization is similar to that seen for α-glucosidase I (α-Glu I; CAZy family GH63 domain) and the sequence-related GH31 α-glucosidase II (α-Glu II; CAZy family GH31 domain), which are two ER enzymes that play essential roles in protein quality control. Through their processing of terminal glucose residues from the *N*-glycans of newly synthesized glycoproteins, these two enzymes serve an essential role in regulating the engagement of glycoproteins within the calnexin/calreticulin cycle(15, 16).

ER α-Glu I and α-Glu II act to cleave α-linked non-reducing glucose residues from a branch of the *N*-glycan, with α-Glu II using a double-displacement mechanism, which involves the transient formation

of a glycosyl enzyme intermediate(17, 18). Based on the sequence similarity of MYORG to α-Glu II (25.2% seq ID; 53% sequence coverage) and conservation of the key catalytic residues, this enzyme has previously been assumed to be a catalytically active α-glucosidase.(11, 19) Yet, attempts to demonstrate the activity of MYORG or identify any substrates for this enzyme have proved unsuccessful.(11) Understanding the substrate specificity of MYORG will help uncover the molecular mechanisms underlying development and progression of PFBC, as well as providing opportunities to design or repurpose existing drugs for treatment. Here, we demonstrate that MYORG, enigmatically, functions not as an α-glucosidase but rather an α-galactosidase and shows marked preference for specific disaccharide substrates. We use X-ray crystallography to obtain unliganded and both substrate and inhibitor bound structures of MYORG. We use these structures to pinpoint how disease-related mutations contribute to loss of function and downstream disease.

Results

MYORG is an active glycoside hydrolase that acts on α-galactosides.

Early efforts to recombinantly express MYORG in *Escherichia coli* proved unsuccessful in generating protein with detectable activity. Given that MYORG resides in the ER lumen and is therefore likely to be *N*-glycosylated, we reasoned that expression in a host system such as the eukaryote *Trichoplusia ni* could lead to active protein. Indeed, extensive glycosylation has previously been observed for MYORG derived from C2C12 cells, for which digestion by the *endo*-glycosidase EndoH, which cleaves *N*-glycans, leads to a ~10 kDa reduction in molecular weight.(11) This sensitivity to EndoH digestion indicates the protein bears high mannose structures, which is consistent with its bearing *N*-glycans as expected of an ER localized protein. To focus on the function of the GH31 domain of MYORG and prevent membrane incorporation, we expressed residues 80-714 (MYORG$_{GH31}$), trimming off the transmembrane domain and the predicted N-terminal disordered region. We also introduced a His$_6$ tag along with a TEV-protease cleavable N-terminal melittin signal sequence to drive secretion of the resulting protein product into the media. In this way, MYORG$_{GH31}$ could be successfully purified from the media using metal-chelate affinity purification. To confirm glycosylation of MYORG, we treated the protein with EndoH and compared both the glycosylated and deglycosylated enzyme through size-exclusion chromatography multi-angle light scattering (SEC-MALLS). Complete digestion by EndoH was monitored through SDS-PAGE (**Figure S1**). SEC-MALLS analysis suggested MYORG$_{GH31}$ is 158 kDa in solution, which is close to the expected molecular weight of a dimer (154 kDa) (**Figure 2a**), whereas deglycosylated MYORG$_{GH31}$ forms a 153 kDa complex, suggesting that glycosylation is not essential for dimerization and that MYORG$_{GH31}$ is decorated with ~5 kDa of *N*-glycans. The relatively high level of *N*-glycosylation likely explains why previous efforts to express this protein in *E.coli* yielded apparently inactive protein.

With suitably folded and expressed MYORG$_{GH31}$ we next analyzed whether this protein showed any activity against α-glucosides including standard chromogenic glucosides such as *para*-nitrophenyl α-D-glucopyranoside and the more sensitive fluorogenic 4-methylumbelliferyl α-D-glucopyranoside (4MU-Glc). However, we observed no activity against these substrates and therefore screened a panel of different 4-methylumbelliferyl (4-MU) α-glycoside substrates including; α-D-mannopyranoside (4MU-Man), α-D-xylopyranoside (4MU-Xyl), α-D-galactopyranoside (4MU-Gal), and *N*-acetyl-α-D-galactosaminide (4MU-GalNAc) (**Figure 2b**). Substrate turnover was only observed for 4MU-Gal, suggesting that MYORG functions as an α-galactosidase. While we were unable to determine full kinetic parameters for 4MU-Gal, due to limited solubility of the substrate, we determined the value of the second-order rate constant k_{cat}/K_M by linear regression of the Michaelis-Menten plot to be 434.8 ± 3.82 M^{-1} min^{-1} (**Figure S2**). Though the enzyme shows apparent complete specificity for α-

galactosides, this second-order rate constant for a highly activated substrate with an excellent activated phenolic leaving group is low. Though purified MYORG$_{GH31}$ showed no bands other than MYORG, the low k$_{cat}$/K$_M$ value we observed left us concerned about the possibility that a low-level contaminant might be giving rise to this α-galactosidase activity. We therefore produced mutant protein in which the predicted general acid/base catalytic residue was mutated (Asp520Asn), which by analogy to other α-glycosidases from GH31(20), should greatly reduce activity if MYORG$_{GH31}$ is responsible for the observed catalysis. Reassuringly, this mutant MYORG$_{GH31}$ failed to turn over 4MU-Gal indicating that MYORG is indeed an α-galactosidase (**Figure 2b**). Since MYORG is naturally glycosylated in cells, we only tested the recombinantly produced glycosylated form in kinetic assays.

We speculated that the low k_{cat}/K_M value we observed for MYORG with 4MU-Gal might be explained by it having an unusual pH optimum for activity. Using 4MU-Gal we found, however, that MYORG has a relatively broad pH-activity profile with optimal activity at pH 6 (**Figure S2**). Accordingly, the lack of any curvature in the Michaelis-Menten plot, coupled with the low k_{cat}/K_M value we observed, suggested to us that the 4MU leaving group compromised substrate binding and resulted in what must be a very high K_M value for this substrate. To further probe the specificity of MYORG, we reasoned that, as a GH31 α-galactosidase, MYORG should bind and be inhibited by deoxynojirimycin analogues, given that deoxynojirimycin itself binds to GH31 *Mus* musculus (*Mm*) α-Glu II with a IC_{50} value of 11.4 µM (21). We therefore reasoned that deoxygalactonojirimycin (DGJ), which is clinically approved as the pharmacological chaperone Migalastat that helps mutant forms of the GH27 α-galactosidase GalA that are found in Fabry disease patients to fold more efficiently and traffic to the lysosome (22, 23), should bind similarly well to MYORG. Consistent with this view, we observed inhibition of MYORG activity towards 4MU-Gal in the presence of DGJ (**Figure S2**). We then used isothermal titration calorimetry to determine a K_D value of 1.33 ± 0.45 µM for binding of DGJ to MYORG$_{GH31}$ (**Figure 2c**). Notably, the observation that MYORG$_{GH31}$ binds tightly to DGJ lends further support for MYORG functioning as an α-galactosidase and also suggests the 4MU leaving group may hinder substrate binding to this enzyme.

Aryl glycosides are sometimes poor substrate for glycoside hydrolases because there exists a +1 binding site on the reducing side of the scissile bond that has a distinct preference for a carbohydrate residue(24). We therefore set out to screen various disaccharide substrates to discern the substrate preference of MYORG. We elected to examine all of the α-galactose containing disaccharide structures that are known to exist in humans including; Gal-α1,3-Gal, Gal-α1,3-GalNAc, and Gal-α1,4-Gal. Surprisingly, using sensitive capillary electrophoresis analyses, we found that none of these substrates were significantly processed by MYORG (**Figure 2d**). We therefore turned to screening of available disaccharides containing a non-reducing α-galactoside (**Figure 2d**) and found of these that Gal-α1,6-Gal was processed to some extent but Gal-α1,4-Glc was cleaved most efficiently. To assess the catalytic proficiency of MYORG on this disaccharide, we performed more detailed kinetic analysis and were able to observe Michael-Menten kinetics (**Figure 2e**) that yielded values for K_M (980 ± 7 µM), k_{cat} (0.047 ± 0.003 min^{-1}), and k_{cat}/K_M (49 ± 7 M^{-1} min^{-1}). Despite the glucose leaving group having a far worse leaving group (pK_a ~ 15)(25) as compared to 4-MU (pK_a ~ 7.8), this second order rate constant measured for Gal-α1,4-Glc is similar to that measured for 4-MU-Gal. Given these collective observations, we were intrigued by the unusual substrate specificity of MYORG and set out to solve the structure of this enzyme.

The X-ray structure of MYORG shows it is a membrane-bound dimer
Given the activity of MYORG towards α-galactosides, we set out to obtain structural insights into active site architecture to understand the molecular basis for the substrate selectivity of MYORG. In

particular, we wanted to observe how differences between the active sites of MYORG and α-Glu II lead to differing substrate preferences, while also attempting to validate our kinetics data by demonstrating how selection of Gal-α1,4-Glc is achieved. We obtained crystals of unliganded MYORG and processed them in the *P*1 space group to 2.43 Å (**Table S2**). The crystal structure was solved by molecular replacement using the *E. coli* GH31 enzyme YicI (PDB: 2F2H) as a search model(26). Four copies of MYORG could be placed within the asymmetric unit (Chains A-D, **Figure S3**). For chains A-C, the polypeptide backbone could be confidently traced into the electron density map, with only the first 11 amino acids (80-91) and two short loop regions (residues 165-171 and 270-276) proving too disordered to model. The N-terminal β-sheet domain of chain D proved more challenging to build and residues 80-99 and 120-143 were omitted from the model due to disorder. Chain C represents the most complete model of MYORG and will be used hereafter to describe the structure of MYORG$_{GH31}$.

Analysis of the crystal structure reveals MYORG is comprised of an antiparallel β-sandwich N-terminal domain (residues 92-287), a (β/α)$_8$-barrel catalytic domain (residues 288-633) with an insertion between α3 and α4 (residues 393-436), and a proximal β-sheet domain (residues 634-714) (**Figure 3a,b**). Five cysteine residues are present in the structure and form two disulphide bonds within the N-terminal domain (C125 with C134 and C158 with C284). DALI analysis on the isolated MYORG GH31 domain reveals greatest similarity with the *Cellvibrio japonicus* α-transglucosylase Agd31B (PDB: 5NPC, Z-score 35.1, 24% sequence identity). Unlike other eukaryotic GH31 family structures, MYORG has an elongated α8 due to formation of a π-helix turn whereas usually a single residue linker connects α8 to the following α-helix. MYORG lacks the common distal C-terminal domain (residues 828-966 in α-Glu II), which is common in GH31 enzymes and forms a large part of the dimerization interface in the α-Glu II heterodimer.

MYORG$_{GH31}$ is predicted to have six *N*-glycosylation sites: N240, N250, N346, N372, N398, and N511. Glycosylation is observed on every polypeptide chain in the asymmetric unit, and it is possible to model *N*-glycans on all of the predicted *N*-glycosylation sites of Chain B and C (**Figure 3a,b**). The observed glycans vary in both their length and glycosylation patterns. Fucose is present linked α1,3 and α1,6 to the reducing end GlcNAc of the N372 glycan, where the former α1,3 linkage is an artefact of insect cell expression. The glycans likely extend further than can be reliably modelled, since positive difference electron density can be observed where additional residues of longer glycan chains would be found. Additional crystal contacts are likely afforded by some of these glycans, for instance, difference density emerging from glycosylated N372 within Chain B and C appears to bury itself in the symmetry-related chain B and C, respectively (**Figure S3**). Notably, numerous additional unassigned peaks in the difference map exist on the surface of the protein structures that are separated from one another by ~5.5 Å. These peaks are incompatible with bound water or molecules present in the crystallization conditions and may therefore represent other transiently bound glycans extending from other chains.

The crystal structure shows that MYORG forms a two-fold dimeric assembly, agreeing with our SEC-MALLS analysis, with the protein-protein interaction exclusively localised to the insert region (**Figure 3c**). This arrangement is best represented by chains B and C, however, chains A and D also form this homodimer assembly. The interface covers 639 Å^2 and is largely supported through a hydrophobic interaction network composed of F402, V406, L419, L422, and I429, in addition to hydrogen bonding between Y397 to E407. A *N*-glycosylation site lies near the interface (N398) and although modelled glycans do not contribute to this interface, transient interactions made through these glycans may further strength the interface. While the MYORG$_{GH31}$ construct lacks the transmembrane domain and the N-terminal disordered domain, the positioning of the N-termini in relation to the dimer interface

suggests the multimeric state is unlikely to be disrupted by incorporation into a membrane. Indeed, the dimer interface can be used to indicate how MYORG sits in the membrane, PSIPRED, DISOPRED, and MEMSAT analysis coupled with the crystallography data suggests only residues 88-91 are disordered, thus the catalytic domain must be angled such that its longest axis is perpendicular to the membrane (**Figure. 3c**).(27-29)

Using the superimposition of MYORG onto α-Glu II (**Figure 3d**; RMSD of 2.35 Å over 495 amino acids; PDB: 5H9O) we were able to validate residues we had tentatively assigned as the nucleophile (D463) and general acid (D520) based on sequence alignments and consensus motifs (**Figure S4**). Comparing the active site of MYORG against Mmα-Glu II it is evident why MYORG is unable to accommodate glucose in the -1 subsite (**Figure 3d**). Specifically, Mmα-Glu II provides a space between W423 and H698 in which the 4-OH of a glucose residue can fit and hydrogen bond with H698. Whereas within the active site of MYORG, the comparable residue, W321, is positioned differently and occupies this space in a manner that would make binding of a glucose residue result in a steric clash between this residue and the 4-OH of glucose. Conversely, Mmα-Glu II is unable to accommodate galactose since its 4-OH would clash with W562. The equivalent residue in MYORG is K461 which would not clash and instead would likely provide a stabilising hydrogen bond.

MYORG selectively binds α-galactosides and its substrate Gal-α1,4-Glc

To visualise how MYORG binds to DGJ, we soaked the inhibitor into crystals of wildtype MYORG$_{GH31}$. Data was collected and processed to 2.43 Å (**Table S2**). Strong positive F_o-F_c difference density was observed in the active sites of all chains in the asymmetric unit, and DGJ was unambiguously modelled within this density in a $^4C_1$ conformation (**Figure 3e; Figure S3**). This conformation is that expected for Michaelis complexes of substrates bound to GH31 family enzymes(26) as well as, based on the structure of the $Chaetomium$ $thermophilum$ α-Glu II, for deoxynojirimycin itself(30). MYORG makes several contacts with DGJ (**Figure 3e**). The general catalytic acid/base residue (D520) of MYORG contacts the 2-OH of DGJ, as does R504 and R517. Further interactions include hydrogen bonds between K461 and the 3-OH of DGJ, D353 with the 4-OH, and D354 and W426 with the 6-OH. The catalytic nucleophile (D463) forms a close, likely ionic interaction, with the endocyclic nitrogen of DGJ (2.59 Å). As inferred from the superimposition of MYORG onto Mmα-Glu II, W321 conveys specificity for galactose through its position, which would clash with the 4-OH of a glucose, mannose, or xylose unit bound in the same position (**Figure 3e**). Furthermore, the structure of the MYORG$_{GH31}$ active site explains why we find 4-MU-GalNAc, despite being galactose-configured, is not a substrate. The N-acetyl group would need to occupy the space in which the general catalytic acid residue and residues R504 and R507 are found. Indeed, the structure of the GH31 family enzyme, Nag31A from $Enterococcus$ $faecalis$ reveals a hydrophobic pocket is required in the area occupied by MYORG R504 and R507 to provide space for the GalNAc methyl group(31). These data provide clear structural support for the strict substrate preference of MYORG for α-galactosides.

To observe how MYORG$_{GH31}$ derives its selectivity for Gal-α1,4-Glc, we set out to capture a Michaelis complex with this disaccharide. We used a catalytically impaired variant of MYORG in which the general acid catalytic residue was conservatively mutated (D520N) to allow the intact substrate to bind stably within the active site. After obtaining crystals of this mutant enzyme, we performed ligand soaking experiments. These experiments ultimately yielded structures with unambiguous F_o-F_c electron density for the substrate (**Figure S3**). Galactose in the -1 subsite is bound in the same position and $^4C_1$ conformation as seen for DGJ, with hydrogen bonding partners being identical other than the endocyclic nitrogen and D520 being swapped for oxygen and N520 (**Figure 3f**). Since the wildtype protein binds to DGJ, and the D520N mutant binds to Gal-α1,4-Glc in a near identical manner, we can

be confident this is the interaction network the wildtype protein uses to bind Gal-α1,4-Glc during catalysis. The glucose residue bound in the +1 site is held in position through hydrogen bonding interactions to D213 and R504, while stacking interactions between the pyranose ring of the glucose residue and W426 likely serve to increase the overall affinity for Gal-α1,4-Glc towards MYORG.

Currently only one other family GH31 α-galactosidase structure is available, that of *Pedobacter saltans* Pedsa_3617 (*Ps*Gal31A; PDB code 4XPO)(24). *Ps*Gal31A uses a similar positioned tryptophan (W486) to W321 to provide specificity for α-galactosides. However, the W486 of *Ps*Gal31A is positioned on a loop between β8 and α8 of the (β/α)$_8$-barrel fold, whereas MYORG W321 is located on a loop between β1 (residues 317-319) and α1 (residues 330-342). Other differences include the galactose 6-OH being coordinated by D354 in MYORG whereas *Ps*Gal31A uses Y274. Additional support is provided to the 2-OH by R517 in MYORG, for which the equivalent residue in *Ps*Gal31A, Y432, is by contrast not positioned to form bonds with the substrate. In the +1 subsite, R504 of MYORG is conserved with R418 of *Ps*Gal31A, however, W426 of MYORG is replaced by E366 in *Ps*Gal31A indicating different substrate preferences. Notably, there is no equivalent residue of D213 in *Ps*Gal31A, which is needed by MYORG to coordinate the 2-OH of glucose. Supporting these observations reflecting a different substrate preference, *Ps*Gal31A has been captured in complex with fucose at the +1 subsite.

To determine why MYORG exhibits specificity for glucose at the +1 subsite over natural disaccharides we performed docking experiments using AutoDock Vina (32). Docked Gal-α1,4-Glc exhibits an almost identical position to Gal-α1,4-Glc in the crystal complex validating our docking procedure and search area (**Figure 4a**; **Figure S5**). This same search area and settings were used to dock in other disaccharides. The most favourable position predicted for natural disaccharides placed the galactose residue at the -1 subsite in a near identical conformation as seen for Gal-α1,4-Glc, further validating the docking methodology (**Figure 4b-e**). These docking studies show known disaccharides can be accommodated in the active site, however, binding of these is poor compared to glucose due to resulting steric clashes imposed by D213, W321, W426 and R504, which forced these other sugars into conformations wherein only single hydrogen bonds are formed and stacking interactions with W426 are disrupted. This reinforces our kinetic observations that currently known human substrates are unlikely to be acted upon by MYORG. In summary, the shape of the +1 subsite dictates specificity for α1,4-Glc since alternative linkages and monosaccharides bound in this site would form unproductive steric clashes.

Structural mapping of PFBC-associated mutations

Numerous PFBC disease-associated mutations are found within *MYORG*. We mapped these mutations onto the structure of MYORG$_{GH31}$ and, using this model, we suggested a mechanism by which each mutation may drive disease development (**Table S1**). While many of these mutations result in protein truncations, frameshifts, deletions, and insertions, several missense mutations are known that resulted in single amino acid changes (**Figure 5a**). Interestingly, two missense mutants (M35V, M35K) are found within the domain extending into the cytoplasm/nucleoplasm (**Table S1**) and are unlikely to affect the catalytic region. As these mutations cause disease progression it is evident that this N-terminal section is essential for homeostasis, however, how mutations of this residue lead to disease is unknown. Of the set of known mutations, only R504P has a clear impact on the active site. This mutant likely leads to loss of stabilising interactions to substrates at the -1 site and thereby disrupts substrate binding (**Figure 3**). However, introduction of a proline at this site might also cause general protein misfolding. By analogy to the many disease-associated missense mutations known to occur within various lysosomal glycoside hydrolases(33, 34), other missense mutations within MYORG, including those located in the ER lumen, may lead to loss of MYORG function by causing its misfolding

(**Table S1**). Such missense mutations that cause misfolding may be amenable to treatment using small molecule pharmacological chaperones. Pharmacological chaperones have shown promise for stabilizing mutant glycoside hydrolases and helping them to mature within the ER and traffic to lysosomes, as seen for the treatment of Fabry disease using DGJ (Galafold)(22, 35). However, stabilization of proteins that are ultimately retained within the ER by promoting their proper folding and escape from the quality control pathway may also be possible. In this regard, we tested whether DGJ could stabilize MYORG, we used a thermal shift assay and found a ΔT_m of 4.4 °C (**Figure 5b**). These results are in keeping with observations made using pharmacological chaperones for lysosomal enzymes and indicate that suitable chaperones may be able to promote correct folding of missense mutants of MYORG. Collectively, these observations suggest the clinically approved DGJ should be explored as a treatment option for patients with MYORG missense mutations. Such a therapy may prevent misfolding of MYORG within the ER, which could block ER-associated degradation of the mutant enzyme and increase its levels to hinder disease progression.

Discussion

The recognized link between autosomal recessive mutations in MYORG and primary familial brain calcification has stimulated increasing interest in the molecular function of this GH31-containing membrane protein. The range of mutations, which include both nonsense and missense mutations (**Table S1**), suggests that loss of function of MYORG, rather than a gain of toxicity leads to PFBC. The sequence similarity of MYORG to the GH31 ER α-Glu II, particularly the high level of conservation of residues in the enzyme active site, coupled with their shared ER localization,(6) has led to the expectation that MYORG is an α-glucosidase(11, 19) and annotation of the MYORG homologue in *Drosophila* (TOBI) as an α-glucosidase.(19) Expression of a site-directed mutant, in which the conserved active site nucleophile residue is varied, in place of the wild-type enzyme has shown that intact catalytic machinery within MYORG is needed for a normal cellular phenotype within myoblasts.(11) Showing that MYORG possesses catalytic activity has, however, been unsuccessful.

Using several lines of structural and biochemical analyses, here we report the surprising observation that MYORG is an α-galactosidase. Since MYORG$_{GH31}$ and TOBI share high sequence ID (86 % query cover, 35 % sequence identity) and structural conservation of the active site, we believe TOBI is also likely to function as a α-galactosidase, as are orthologues found within other metazoans. Moreover, the conservation of MYORG among metazoans suggests an evolutionarily conserved function, which has yet to be uncovered. From a functional perspective, within *Drosophila*, *tobi* expression is regulated by both insulin-producing cells and cells comprising the corpora cardiaca though insulin-like peptides and the insect glucagon homolog, adipokinetic hormone, which suggests a link between *tobi* and insulin signalling.(19) Indeed, expression of *tobi* can be modulated through dietary proteins and sugars, with high protein food leading to an increase in *tobi* expression, whereas high sugar food represses its expression. Reducing *tobi* expression decreases the life span of *Drosophila* on high protein food, and it is interesting that overexpression of *tobi* in flies fed a high sugar diet leads to severe growth defects and decreases in body glycogen.(19) However, the link, if any to development of PFBC in humans is unclear.

Previous functional studies on MYORG demonstrate involvement in secretion of insulin growth factor II (IGF-II) with the suggestion that MYORG interacts with pro-IGF-II(11). Pro-IGF-II is known to be extensively *O*-glycosylated(36, 37). These observations suggested to us the possibility that MYORG might be involved in processing an α-galactosidic linkage within glycoproteins. The only two α-

galactoside-containing glycans found to this date on glycoproteins within humans are Gal-α1,3-GalNAc that comprises the Core8 structure found in O-glycans and Gal-α1,3-Gal found within blood group antigen B. In addition, the globosides Gb2 (Gal-α1,4-Gal) and Gb3 (Gal-α1,4-Gal) are also found in humans. None of these disaccharides, however, are turned over by MYORG (**Figure 2d**). Our X-ray structure data reveals features of the MYORG active site that explain why none of these α-galactosides are turned over by this enzyme. In particular, the binary substrate complex of MYORG bound to Gal-α1,4-Glc explains both its requirement for galactosides binding within the -1 subsite and strong preference for glucose binding within the +1 binding site. Strategically positioned residues within the active site exclude the possibility of other monosaccharides binding to either of these subsites within MYORG. This substrate selectivity for Gal-α1,4-Glc is striking because glycans containing this disaccharide are currently unknown within humans. Based on these collective observations, we posit that the Gal-α1,4-Glc structure is yet to be found within the ER of mammals, where we expect it might fulfil roles in protein quality control.

The structure of the GH31 domain of MYORG enabled us to confidently map PFBC-associated mutations in MYORG. Among the 46 known disease-associated MYORG mutations, 22 are missense mutations and these can be found widely distributed throughout its GH31 domain. That such mutations, some of which are quite conservative, such as G286S and I656T, give rise to PFBC is reminiscent of the lysosomal storage diseases, where many missense mutations have been found that impair protein maturation and proper trafficking to lysosomes.(38, 39) Notable in this regard is that active site ligands that bind to lysosomal enzymes(40) stabilize these proteins and facilitate their proper folding and trafficking to lysosomes. Several iminosugars have been explored as candidate therapeutics, with several having entered into the clinic.(22) Significantly, DGJ (migalastat) is clinically approved (Galafold) as a chemical chaperone for the lysosomal α-galactosidase encoded by *GLA*. We found that DGJ both bound to MYORG with reasonable affinity (K_D = 1.33 μM) and stabilized this protein against thermal denaturation. These observations raise the possibility that migalastat could be repurposed for MYORG patients having missense mutations that could be stabilized by a pharmacological chaperone. Accordingly, a logical next step will be to examine the stability of MYORG variants containing PFBC-associated missense mutations and assess the potential for migalastat to stabilize and help folding of these mutant proteins.

Finally, with regard to how MYORG contributes to PFBC, the ER localization of MYORG, coupled with its now established glycosidase activity and similarity to ER α-Glu II, makes it tempting to suggest that dysfunction of MYORG as seen in PFBC, may arise because of a role in quality control where it may regulate the folding or maturation of one or more of the protein products of genes linked to PFBC including *SLC20A2*, *PDGFB*, *PDGFRB*, and *XPR1*(2-5). Notably, all of the products of these PFBC-linked genes are glycoproteins, and glycan processing is known to be essential for the proteolytic processing of beta subunit of platelet-derived growth factor (PDGFB)(41). Interestingly, MYORG is only one of two PFBC-associated genes that is associated with an autosomal recessive form of this disease, the other being JAM2(6, 7), which suggests its enzymatic activity is essential to avoid downstream development of PFBC. Given these observations, a logical path forward will be to assess the effects of loss of MYORG function on the production and activity of these PFBC-associated proteins.

Materials and Methods
Construction of wildtype and mutant MYORG expressing baculovirus
MYORG cDNA (Genscript) encoding residues 80-714 (UniProt: Q6NSJ0-1, starting V^{80}SLRK) was amplified and inserted into a modified pOMNIBac plasmid (encoding N-terminal TEV protease cleavable 6xHis-tag and honey-bee melittin signal sequence)(42) by sequence and ligation

independent cloning(43, 44). Mutants of MYORG were produced using the Q5® site-directed mutagenesis kit as per manufacturer's instructions. Recombinant bacmid was produced using a Tn7 transposition protocol in DH10EMBacY cells (Geneva Biotech)(45, 46). Bacmid was subsequently purified using a PureLink™ HiPure Plasmid Miniprep kit (Invitogen) by manufacturer's instructions. To produce the V1 baculovirus stock, 6 x 2 ml volumes of 0.45 x 10^6 cells/ml SF9 cells were each incubated statically at 28 °C with 180 µl of transfection mastermix (1050 µl Insect-XPRESS™ media (Lonza), 38 µl of bacmid at ~60 ng/µl, and 31.5 µl FuGENE® HD transfection reagent (Promega)) until cells were 95 % fluorescent (~2 days). Cells and debris were removed by centrifugation at 200 g for 5 min. Fetal bovine serum was added to the clarified solution to a final concentration of 2 %. To produce the V2 stock, 1 ml of V1 stock was added to 50 ml of SF9 cells at 1 x 10^6 cells/ml and cells were incubated at 28 °C with shaking until 95 % fluorescent. Cells and debris were removed by a 5 min centrifugation at 200 g. Fetal bovine serum was added to a final concentration of 2 % to clarified conditioned media and this solution was used hereafter as the V2 stock.

Protein expression and purification of wildtype and mutant MYORG

High Five cells (*Trichoplusia ni*) were grown to confluence of 2 x 10^6 cell/ml (total 3.6 litres) in Gibco Express Five™ SFM media supplemented with 18 mM L-Glutamine before transfection with 1 ml of V2 per 600 ml of culture. At >50 % cell viability and >95 % fluorescence, cells and debris were removed by a two-step centrifugation at 4 °C, the first at 55 g for 20 mins and a second at 5500 g for 20 mins. Conditioned media was supplemented with AEBSF (to 0.1 mM final) and imidazole (to 40 mM final). For crystallography, conditioned media was loaded onto a 5 ml HisTrap Excel column (GE Healthcare) equilibrated in buffer A (20 mM HEPES pH 7.5, 200 mM NaCl, 40 mM imidazole and 1 mM DTT) and eluted by a stepwise gradient of buffer B (as buffer A except 400 mM imidazole) in buffer A. Fractions containing protein were pooled and diluted 1 in 10 with 20 mM HEPES pH 7.5, 200 mM NaCl and 1 mM DTT before being treated 1:50 with TEV protease overnight at 4 °C. Protein sample was passed over a 5 ml HisTrap Excel column equilibrated in buffer A and the flow through was concentrated using a Vivaspin® centrifugal concentrator (Sartorius) and size excluded on a 16/600 Superdex 200 column (GE Healthcare) in 20 mM HEPES pH 7.5, 200 mM NaCl and 1mM DTT. Protein was concentrated as before and snap frozen in liquid nitrogen.

For kinetic analysis, protein purification was modified slightly to improve purity, buffer A was swapped with buffer C (20 mM MES pH 6.4, 200 mM NaCl, 40 mM imidazole and 1 mM DTT) and buffer B exchanged for buffer D (as buffer C except 400 mM imidazole) for the His-tag purification. Fractions containing MYORG were pooled and dialysed overnight at 4 °C with 1:50 TEV protease against 20 mM MES pH 6.4, 50 mM NaCl and 1mM DTT. Dialysed samples were passed over a 1 ml HiTrap SP HP cation ion exchange column (GE Healthcare) and eluted from the column by a stepwise gradient of 20 mM MES pH 6.4 up to 20 mM MES 6.4 and 1 M NaCl. Fractions containing protein were pooled, concentrated as previously and snap frozen in liquid nitrogen. Purity of samples was accessed by SDS-Page and western blot.

Kinetics using 4MU-Gal

Measurements were carried out in a 96 well black bottomed plate using a CLARIOstar plus plate reader. Assays was carried out at 25 °C in a total reaction volume of 100 µl composed of reaction buffer (20 mM HEPES pH 7.5, 200 mM NaCl, 1 mM DTT, 0.1% BSA) and 100 µM of substrate. Reaction was initiated with a final concentration of 100 nM recombinant MYORG protein in reaction buffer, or reaction buffer only for the controls. Reaction was stopped at timepoints by adding 5 µl of reaction mix to 100 µl of stop buffer (reaction buffer adjusted to pH 10.4). Endpoint 4-methylumbelliferyl release was detected by measuring absorbance (360 nm excitation and 450 nm emission). Each

reaction was run in doublet and measurements averaged. Three technical repeats were carried out for each reaction under investigation. For the pH profile, enzyme at 50 nM was assayed in 50 mM phosphate-citrate buffer (pH 5.0 to pH 8.0), 200 mM NaCl, 1 mM DTT, 0.1 % BSA at 25 °C. To calculate k_{cat}/K_M, enzyme at 50 nM was assayed in 20 mM MES pH 6.5, 200 mM NaCl, 1 mM DTT, 0.1 % BSA and 2% DMSO using a substrate range of 2 mM to 31.25 μM (2-fold serial dilution) at 37 °C. All rates were linear over the time course. Activity of MYORG ± DGJ was assayed in 20 mM MES 6.5, 200 mM NaCl, 1 mM DTT, 0.1% BSA at 25°C ± 10 μM DGJ. For pH, Michaelis-Menten kinetics, and MYORG ± DGJ assays, timepoints were taken by mixing 5 μl of reaction with 45 μl of 1 M Glycine pH 10.

Substrate reduction assays

The substrate scope of MYORG was assessed using the following oligosaccharides, all of which were used as received: 4-*O*-α-D-galactopyranosyl-D-glucopyranose (*i.e.* Gal-α1,4-Glc), Gal-α1,3-Gal, Gal-α1,4-Gal and Gal-α1,6-Gal, were purchased from Synthose Inc. (Concord, ON, Canada); blood group B trisaccharide (Gal-α1,3-Gal(Fuc-α1,2)), core-8 *O*-glycan (Gal-α1,3-GalNAc), and 2'-fucosyllactose (2'FL) were obtained from Biosynth International, Inc. (San Diego, CA, USA). Stocks of all substrates were prepared in 18 MΩ·cm water and stored at -20 °C until use. 25 nmol of each di- or trisaccharide was mixed with 2.87 μM MYORG in 50 mM HEPES, pH 7.4, containing 50 mM NaCl and 0.025% BSA; 20 nmol 2'FL, as an internal standard, was included in all reactions. After incubating at 37 °C overnight, all reactions were immediately loaded onto 250 mg Supelco ENVICarb solid phase extraction (SPE) cartridges (Sigma) that had been preconditioned by washing with 3 mL 80% methanol followed by 3 x 3 mL water. Salts and monosaccharides were washed off the SPE cartridge with water (3 mL) before any remaining oligosaccharides were eluted with 50% acetonitrile (2 x 2.2 mL). Eluted material was pooled, partially concentrated using a SpeedVac (Thermo) and lyophilized in 200 μL tubes. Samples were fluorescently labelled using 8-aminopyrene-1,3,6-trisulfonate (APTS) and analyzed by capillary electrophoresis with laser-induced fluorescence detection (CE-LIF) exactly as previously described(47). Several representative electropherograms are depicted in **Figure S6**. CE-LIF peak areas for all substrates were corrected against the 2'FL internal standard, and all peak ratios were subsequently normalized such that those to which no MYORG had been added were adjusted to 100%.

Paired-enzyme assay

The kinetic parameters of MYORG against the disaccharide substrate 4-*O*-α-D-galactopyranosyl-D-glucopyranose (Gal-α1,4-Glc) were established using a glucose oxidase (GOX) and horseradish peroxidase (HRP; both from Sigma) paired-enzyme assay. The reactions were performed in a 0.1 M sodium phosphate buffer, pH 7.0. Each reaction mixture consisted of 2.25 mM 2,2'-azino-bis(3-ethylbenzothiazoline-6-sulfonic acid) diammonium salt (ABTS; Sigma), 5.40 U/mL HRP, 15.30 U/mL of GOX and 80 nM MYORG. The substrate concentration was varied between 0 and 1200 μM. Reactions were initiated by adding the MYORG, mixed for 2 min, and the absorbance at 575 nm was recorded at 30 s intervals over 1 h using a BioTek Epoch Microplate Spectrometer (Fisher Scientific) incubated at 25 °C. Analysis was done by plotting the absorbance as a function of time in seconds. The slope for the plot (*i.e*. change in absorbance with time) was calculated within the range of 15 min (900 s) to 40 mins (2400 s) for each substrate concentration. The change in rate was then plotted against the substrate concentration to determine the estimated K_M and V_{max} of MYORG.

Structure Determination

MYORG at 10.5 mg/ml was screened against the index HT screen (Hampton Research) and diffraction quality crystals were obtained in 100 mM HEPES pH 7.0, 10% PEG MME5000 and 5% tasimate pH 7.0. Highest quality crystals were obtained by increasing the drop size to 3 μl (1:1 ratio protein to reservoir) and using a cat whisker to streak seed a crystal seed stock made from the same condition through it.

Apo-crystals were cryoprotected in mother liqueur supplemented with 20 % ethylene glycol and flash cooled in liquid nitrogen. For DGJ complexed crystals, crystals were soaked for 4 hours in the same cryoprotectant supplemented with 10 mM DGJ. For the Gal-α1,4-Glc complex, D520N mutant MYORG crystals were soaked with 10 mM Gal-α1,4-Glc (Biosynth International, Inc). Diffraction data were collected at Diamond Light Source in Oxford, UK. Data reduction and processing was completed through DIALS and AIMLESS (48, 49). A structure solution was obtained through PHASER (50) using PDB code 2F2H as a search model after improvement using CHAINSAW(51). PHENIX AutoBuild was used to correct the sequence register in the catalytic domain by rebuilding(52). Modelling the N-terminal domain and final cycles of refinement were completed through iterative cycles of interactive building in coot and refinement in REFMAC(53, 54). Geometric restraints for DGJ were generated through eLBOW(55). Restraints and validation of glycans were performed though Privateer (56). Figures were produced in ChimeraX(57). AutoDock Vina was used to dock substrates into the active site (32). As the highest resolution structure and with residues primed for substrate binding, chain B of the MYORG complex with Gal-α1,4-Glc was used for docking. Before docking, N520 was reverted to D520.

SEC-MALLS

SEC-MALLS analysis was conducted on a system comprising a Wyatt HELEOS-II multi-angle light scattering detector and a Wyatt rEX refractive index detector linked to a Shimadzu HPLC system (SPD-20A UV detector, LC20-AD isocratic pump system, DGU-20A3 degasser and SIL-20A autosampler). Experiments were conducted at ambient temperature. For protein separation, a Superdex S200 10/300 GL column pre-equilibrated in running buffer (20 mM HEPES 7.5, 200 mM NaCl) was used. Sample injection was 100 μl of 3 mg/ml MYORG. Flow rate was set at 0.5 ml/min. Shimadzu LabSolutions software was used to control the HPLC and Astra 7 software for the HELEOS-II and rEX detectors. The Astra data collection was 1 minute shorter than the LC solutions run to maintain synchronisation. Data were analysed using the Astra 7 software and figures created using GraphPad Prism. Molecular weights were estimated using the Zimm fit method with degree 1. A value of 0.182 was used for protein refractive index increment (dn/dc).

Isothermal Titration Calorimetry

ITC measurements were taken on a MicroCal Auto-ITC$_{200}$ calorimeter. Protein was buffer exchanged into DGJ buffer (20 mM HEPES pH 7.0, 200 mM NaCl) using Zeba spin desalting columns, 7K MWCO as per manufacturer's instructions. DGJ (100 μM) was added by syringe into a cell containing MYORG (10 μM) over 20, 2 μl injections (0.5 μl for first injection) at 25 °C. Injections were spaced by 120 secs (180 secs for first injection). Binding affinity was calculated by one site fitting in the MicroCal PEAQ-ITC analysis software. Experiment was run in duplicate.

Thermal Shift Analysis

A 50 μl reaction containing 20 mM MES pH 6.5, 200 mM NaCl, 5 x SYPRO^{TM} orange protein dye and 2.5 μM MYORG ± 50 μM DGJ was incrementally raised from 24 °C to 94.6 °C using a Stratagene Mx3005P qPCR system. Fluorescence was detected by excitation at 517 nm and emission at 585 nm. Three technical repeats were performed for each condition. Repeats were normalised to their maximum fluorescence value. To obtain a T_m value, data points were fitted with a Boltzmann model where points right of the highest value and left of the lowest value were discarded before fitting. GraphPad Prism 5 was used for fitting.

Sequence Alignments

Protein sequences were aligned through Clustal Omega(58) and figures were constructed with ESPript3 (59).

Author Contributions
R.W.M, W.F.Z, G.J.D and D.J.V designed the experiments; R.W.M, J.B., O.B.F. and W.F.Z. performed the experiments; all authors interpreted the results; R.W.M, and D.J.V wrote the manuscript with input from all the authors.

Competing interests
The authors declare no competing interests

Data Availability
Atomic coordinates have been deposited under PDB codes: 7QQF (unliganded), 7QQG (DGJ-bound) and 7QQH (D520N mutant - Gal-α1,4-Glc complex).

References
1.   Nicolas G, Pottier C, Charbonnier C, Guyant-Maréchal L, Le Ber I, Pariente J, et al. Phenotypic spectrum of probable and genetically-confirmed idiopathic basal ganglia calcification. Brain. 2013;136(Pt 11):3395-407.
2.   Keller A, Westenberger A, Sobrido MJ, García-Murias M, Domingo A, Sears RL, et al. Mutations in the gene encoding PDGF-B cause brain calcifications in humans and mice. Nat Genet. 2013;45(9):1077-82.
3.   Legati A, Giovannini D, Nicolas G, López-Sánchez U, Quintáns B, Oliveira JR, et al. Mutations in XPR1 cause primary familial brain calcification associated with altered phosphate export. Nat Genet. 2015;47(6):579-81.
4.   Nicolas G, Pottier C, Maltête D, Coutant S, Rovelet-Lecrux A, Legallic S, et al. Mutation of the PDGFRB gene as a cause of idiopathic basal ganglia calcification. Neurology. 2013;80(2):181-7.
5.   Wang C, Li Y, Shi L, Ren J, Patti M, Wang T, et al. Mutations in SLC20A2 link familial idiopathic basal ganglia calcification with phosphate homeostasis. Nat Genet. 2012;44(3):254-6.
6.   Yao XP, Cheng X, Wang C, Zhao M, Guo XX, Su HZ, et al. Biallelic Mutations in MYORG Cause Autosomal Recessive Primary Familial Brain Calcification. Neuron. 2018;98(6):1116-23.e5.
7.   Schottlaender LV, Abeti R, Jaunmuktane Z, Macmillan C, Chelban V, O'Callaghan B, et al. Bi-allelic JAM2 Variants Lead to Early-Onset Recessive Primary Familial Brain Calcification. Am J Hum Genet. 2020;106(3):412-21.
8.   López-Sánchez U, Tury S, Nicolas G, Wilson MS, Jurici S, Ayrignac X, et al. Interplay between primary familial brain calcification-associated SLC20A2 and XPR1 phosphate transporters requires inositol polyphosphates for control of cellular phosphate homeostasis. J Biol Chem. 2020;295(28):9366-78.
9.   Vanlandewijck M, Lebouvier T, Andaloussi Mäe M, Nahar K, Hornemann S, Kenkel D, et al. Functional Characterization of Germline Mutations in PDGFB and PDGFRB in Primary Familial Brain Calcification. PLoS One. 2015;10(11):e0143407.

10.   Aurrand-Lions M, Duncan L, Ballestrem C, Imhof BA. JAM-2, a novel immunoglobulin superfamily molecule, expressed by endothelial and lymphatic cells. J Biol Chem. 2001;276(4):2733-41.

11.   Datta K, Guan T, Gerace L. NET37, a nuclear envelope transmembrane protein with glycosidase homology, is involved in myoblast differentiation. J Biol Chem. 2009;284(43):29666-76.

12.   Lombard V, Golaconda Ramulu H, Drula E, Coutinho PM, Henrissat B. The carbohydrate-active enzymes database (CAZy) in 2013. Nucleic Acids Res. 2014;42(Database issue):D490-5.

13.   Henrissat B, Davies G. Structural and sequence-based classification of glycoside hydrolases. Curr Opin Struct Biol. 1997;7(5):637-44.

14.   Schirmer EC, Florens L, Guan T, Yates JR, 3rd, Gerace L. Nuclear membrane proteins with potential disease links found by subtractive proteomics. Science. 2003;301(5638):1380-2.

15.   Hammond C, Braakman I, Helenius A. Role of N-linked oligosaccharide recognition, glucose trimming, and calnexin in glycoprotein folding and quality control. Proc Natl Acad Sci U S A. 1994;91(3):913-7.

16.   Peterson JR, Ora A, Van PN, Helenius A. Transient, lectin-like association of calreticulin with folding intermediates of cellular and viral glycoproteins. Mol Biol Cell. 1995;6(9):1173-84.

17.   Frandsen TP, Svensson B. Plant alpha-glucosidases of the glycoside hydrolase family 31. Molecular properties, substrate specificity, reaction mechanism, and comparison with family members of different origin. Plant Mol Biol. 1998;37(1):1-13.

18.   Caputo AT, Alonzi DS, Marti L, Reca IB, Kiappes JL, Struwe WB, et al. Structures of mammalian ER α-glucosidase II capture the binding modes of broad-spectrum iminosugar antivirals. Proc Natl Acad Sci U S A. 2016;113(32):E4630-8.

19.   Buch S, Melcher C, Bauer M, Katzenberger J, Pankratz MJ. Opposing effects of dietary protein and sugar regulate a transcriptional target of Drosophila insulin-like peptide signaling. Cell Metab. 2008;7(4):321-32.

20.   Okuyama M, Okuno A, Shimizu N, Mori H, Kimura A, Chiba S. Carboxyl group of residue Asp647 as possible proton donor in catalytic reaction of alpha-glucosidase from Schizosaccharomyces pombe. Eur J Biochem. 2001;268(8):2270-80.

21.   Sayce AC, Alonzi DS, Killingbeck SS, Tyrrell BE, Hill ML, Caputo AT, et al. Iminosugars Inhibit Dengue Virus Production via Inhibition of ER Alpha-Glucosidases--Not Glycolipid Processing Enzymes. PLoS Negl Trop Dis. 2016;10(3):e0004524.

22.   McCafferty EH, Scott LJ. Migalastat: A Review in Fabry Disease. Drugs. 2019;79(5):543-54.

23.   Guce AI, Clark NE, Rogich JJ, Garman SC. The molecular basis of pharmacological chaperoning in human α-galactosidase. Chem Biol. 2011;18(12):1521-6.

24.   Miyazaki T, Ishizaki Y, Ichikawa M, Nishikawa A, Tonozuka T. Structural and biochemical characterization of novel bacterial α-galactosidases belonging to glycoside hydrolase family 31. Biochem J. 2015;469(1):145-58.

25.   Feng S, Bagia C, Mpourmpakis G. Determination of proton affinities and acidity constants of sugars. J Phys Chem A. 2013;117(24):5211-9.

26.   Kim YW, Lovering AL, Chen H, Kantner T, McIntosh LP, Strynadka NC, et al. Expanding the thioglycoligase strategy to the synthesis of alpha-linked thioglycosides allows structural investigation of the parent enzyme/substrate complex. J Am Chem Soc. 2006;128(7):2202-3.

27.   Buchan DWA, Jones DT. The PSIPRED Protein Analysis Workbench: 20 years on. Nucleic Acids Res. 2019;47(W1):W402-w7.

28.   Jones DT, Cozzetto D. DISOPRED3: precise disordered region predictions with annotated protein-binding activity. Bioinformatics. 2015;31(6):857-63.

29.   Nugent T, Jones DT. Transmembrane protein topology prediction using support vector machines. BMC Bioinformatics. 2009;10:159.

30.   Satoh T, Toshimori T, Yan G, Yamaguchi T, Kato K. Structural basis for two-step glucose trimming by glucosidase II involved in ER glycoprotein quality control. Sci Rep. 2016;6:20575.

31.   Miyazaki T, Park EY. Crystal structure of the Enterococcus faecalis α-N-acetylgalactosaminidase, a member of the glycoside hydrolase family 31. FEBS Lett. 2020;594(14):2282-93.

32.   Trott O, Olson AJ. AutoDock Vina: improving the speed and accuracy of docking with a new scoring function, efficient optimization, and multithreading. J Comput Chem. 2010;31(2):455-61.

33.   Platt FM, d'Azzo A, Davidson BL, Neufeld EF, Tifft CJ. Lysosomal storage diseases. Nat Rev Dis Primers. 2018;4(1):27.

34.   Ferreira CR, Gahl WA. Lysosomal storage diseases. Transl Sci Rare Dis. 2017;2(1-2):1-71.

35.   Fan JQ, Ishii S, Asano N, Suzuki Y. Accelerated transport and maturation of lysosomal alpha-galactosidase A in Fabry lymphoblasts by an enzyme inhibitor. Nat Med. 1999;5(1):112-5.

36.   Duguay SJ, Jin Y, Stein J, Duguay AN, Gardner P, Steiner DF. Post-translational processing of the insulin-like growth factor-2 precursor. Analysis of O-glycosylation and endoproteolysis. J Biol Chem. 1998;273(29):18443-51.

37.   Jespersen S, Koedam JA, Hoogerbrugge CM, Tjaden UR, van der Greef J, Van den Brande JL. Characterization of O-glycosylated precursors of insulin-like growth factor II by matrix-assisted laser desorption/ionization mass spectrometry. J Mass Spectrom. 1996;31(8):893-900.

38.   Tekin Orgun L, Besen Ş, Sangün Ö, Bisgin A, Alkan Ö, Erol İ. First pediatric case with primary familial brain calcification due to a novel variant on the MYORG gene and review of the literature. Brain Dev. 2021;43(7):789-97.

39.   Forouhideh Y, Müller K, Ruf W, Assi M, Seker T, Tunca C, et al. A biallelic mutation links MYORG to autosomal-recessive primary familial brain calcification. Brain. 2019;142(2):e4.

40.   Parenti G, Andria G, Valenzano KJ. Pharmacological Chaperone Therapy: Preclinical Development, Clinical Translation, and Prospects for the Treatment of Lysosomal Storage Disorders. Mol Ther. 2015;23(7):1138-48.

41.   Kaetzel DM, Jr., Morgan D, 3rd, Reid JDt, Fenstermaker RA. Site-directed mutagenesis of the N-linked glycosylation site in platelet-derived growth factor B-chain results in diminished intracellular retention. Biochim Biophys Acta. 1996;1298(2):250-60.

42.   Vijayachandran LS, Thimiri Govinda Raj DB, Edelweiss E, Gupta K, Maier J, Gordeliy V, et al. Gene gymnastics: Synthetic biology for baculovirus expression vector system engineering. Bioengineered. 2013;4(5):279-87.

43.   Li MZ, Elledge SJ. Harnessing homologous recombination in vitro to generate recombinant DNA via SLIC. Nat Methods. 2007;4(3):251-6.

44.   Thimiri Govinda Raj DB, Vijayachandran LS, Berger I. OmniBac: universal multigene transfer plasmids for baculovirus expression vector systems. Methods Mol Biol. 2014;1091:123-30.

45.   Trowitzsch S, Bieniossek C, Nie Y, Garzoni F, Berger I. New baculovirus expression tools for recombinant protein complex production. J Struct Biol. 2010;172(1):45-54.

46.   Bieniossek C, Imasaki T, Takagi Y, Berger I. MultiBac: expanding the research toolbox for multiprotein complexes. Trends Biochem Sci. 2012;37(2):49-57.

47.   Vicaretti SD, Mohtarudin NA, Garner AM, Zandberg WF. Capillary Electrophoresis Analysis of Bovine Milk Oligosaccharides Permits an Assessment of the Influence of Diet and the Discovery of Nine Abundant Sulfated Analogues. J Agric Food Chem. 2018;66(32):8574-83.

48.   Winter G, Waterman DG, Parkhurst JM, Brewster AS, Gildea RJ, Gerstel M, et al. DIALS: implementation and evaluation of a new integration package. Acta Crystallogr D Struct Biol. 2018;74(Pt 2):85-97.

49.   Evans PR, Murshudov GN. How good are my data and what is the resolution? Acta Crystallographica Section D: Biological Crystallography. 2013;69(7):1204-14.

50.   Bunkóczi G, Echols N, McCoy AJ, Oeffner RD, Adams PD, Read RJ. Phaser.MRage: automated molecular replacement. Acta Crystallogr D Biol Crystallogr. 2013;69(Pt 11):2276-86.

51.   Stein N. CHAINSAW: a program for mutating pdb files used as templates in molecular replacement. Journal of Applied Crystallography. 2008;41(3):641-3.

52.   Liebschner D, Afonine PV, Baker ML, Bunkóczi G, Chen VB, Croll TI, et al. Macromolecular structure determination using X-rays, neutrons and electrons: recent developments in Phenix. Acta Crystallogr D Struct Biol. 2019;75(Pt 10):861-77.

53.   Murshudov GN, Skubák P, Lebedev AA, Pannu NS, Steiner RA, Nicholls RA, et al. REFMAC5 for the refinement of macromolecular crystal structures. Acta Crystallogr D Biol Crystallogr. 2011;67(Pt 4):355-67.

54.   Emsley P, Lohkamp B, Scott WG, Cowtan K. Features and development of Coot. Acta Crystallogr D Biol Crystallogr. 2010;66(Pt 4):486-501.

55.   Moriarty NW, Grosse-Kunstleve RW, Adams PD. electronic Ligand Builder and Optimization Workbench (eLBOW): a tool for ligand coordinate and restraint generation. Acta Crystallogr D Biol Crystallogr. 2009;65(Pt 10):1074-80.

56.   Agirre J, Iglesias-Fernández J, Rovira C, Davies GJ, Wilson KS, Cowtan KD. Privateer: software for the conformational validation of carbohydrate structures. Nat Struct Mol Biol. 2015;22(11):833-4.

57.   Pettersen EF, Goddard TD, Huang CC, Meng EC, Couch GS, Croll TI, et al. UCSF ChimeraX: Structure visualization for researchers, educators, and developers. Protein Sci. 2021;30(1):70-82.

58.   Sievers F, Wilm A, Dineen D, Gibson TJ, Karplus K, Li W, et al. Fast, scalable generation of high-quality protein multiple sequence alignments using Clustal Omega. Mol Syst Biol. 2011;7:539.

59.   Robert X, Gouet P. Deciphering key features in protein structures with the new ENDscript server. Nucleic Acids Res. 2014;42(Web Server issue):W320-4.

Figure Legends

Figure 1. ER lumen α-glycosidases play roles in *N*-glycan processing. Crystal structures of *Mus musculus* α-glucosidase I (PDB: 5MHF) and II (PDB: 5F0E). The transfer of $Glc_3Man_9GlcNAc_2$ onto nascent polypeptide chains initiates an ER localized quality control process wherein the terminal non-reducing α1-2-linked glucose and the two inner α1-3-linked glucose residues are hydrolysed by α-Glu I and α-Glu II, respectively. Retention in the ER of glycoproteins bearing the innermost α1-3-linked glucose by the chaperones calnexin and calreticulin coupled with re-attachment of α1-3-linked glucose to misfolded proteins by UDP-glucose:glycoprotein glucosyltransferase regulates protein quality control. The function of MYORG within the ER and relevance to glycoprotein processing is unknown. The symbols used for monosaccharides follow the recommendations of the Consortium for Functional Glycomics (CFG).

Figure. 2. MYORG is a dimeric α-galactosidase that shows distinct substrate specificity. **a,** SEC-MALLS traces of glycosylated and EndoH-treated MYORG. **b**, Fluorescent activity assay of MYORG against 4MU-α-linked substrates. Data is mean from three technical replicates ± standard deviations. **c**, Example Isothermal titration calorimetry trace of DGJ binding to MYORG. **ci,** raw baseline subtracted injection profile of the ITC experiment. **cii,** titration curve with points in blue and fitted line in black. **d**, Activity screening of MYORG against disaccharides. BGBT, Blood group B trisaccharide. Experiment repeated twice with three technical repeats in each replicate. **e**, Michaelis-Menten kinetics for processing of Gal-α1-4-Glc by MYORG. Data from three technical repeats. All raw data underlying graphs can be found in S1_Data.

Figure 3. MYORG is a membrane bound dimer that selectively binds an unusual Gal-α1,4-Glc epitope. **a,** Domain boundaries of MYORG with numbering representing the last residue of the domain. TMD, transmembrane domain. NTβSD, N-terminal β-sheet domain. PβSD, proximal β-sheet domain. **b**, Cartoon ribbon representation of MYORG with *N*-glycans depicted as sticks with the glycosylated Asn residues labelled. **c,** The MYORG dimer arrangement showing the insert region and the expected orientation of MYORG with respect to the ER membrane based on analyses using PSIPRED(27),

DISOPRED(28), and MEMSAT(29). **d**, Comparison of the active site of MYORG (blue, residue labelling in black) with that of *Mm*α-Glu-II (purple; PDB: 5H9O). D-glucose is bound by *Mm*α-Glu-II and is depicted in pink. **e,** Residues involved in the positioning and binding of DGJ. **f,** Residues involved in binding Gal-α1,4-Glc. Dashed lines in **e** and **f** represent hydrogen bonding. Magenta sticks are used to emphasise the catalytic acid (D520, mutated to N520 in **f**) and nucleophile (D463) residues.

Figure 4. The Gal-α1,4-Glc epitope is preferentially accommodated within the active site of MYORG. **a**, Difference in position of Gal-α1,4-Glc derived from ligand soaking experiments (dark green) from the docked model of Gal-α1,4-Glc (light green). **b-e**, Docked natural disaccharides in the active site of MYORG. Dotted lines represent hydrogen bonding.

Figure 5. Mapping PFBC disease-associated mutations in MYORG and stabilisation of MYORG by DGJ. **a,** Missense mutations of MYORG are depicted in green and R504 is shown as sticks in magenta. DGJ is depicted as balls and sticks. **b,** Boltzmann fit of thermal shift data depicting difference between MYORG alone and MYORG in the presence of DGJ at a 1:20 molar ratio. Results from three technical replicates. All raw data underlying graphs can be found in S1_Data.
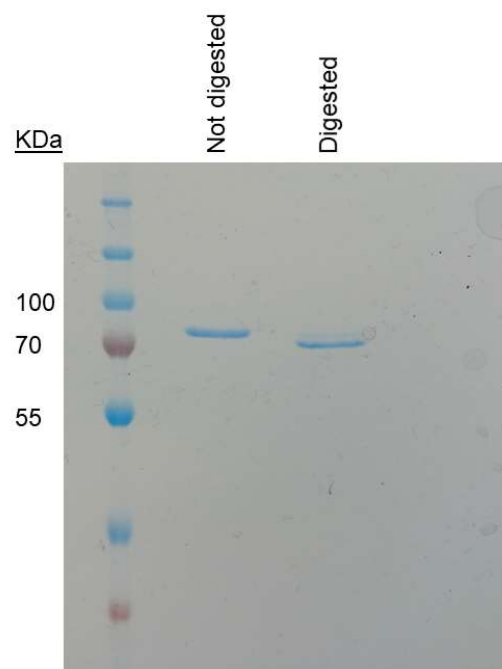
Figure S1. SDS-PAGE gel displaying both fully glycosylated MYORG and MYORG after EndoH treatment. A clear reduction in size is seen upon digestion indicating removal of glycans.

Original unmodified gel picture taken for Figure S1.
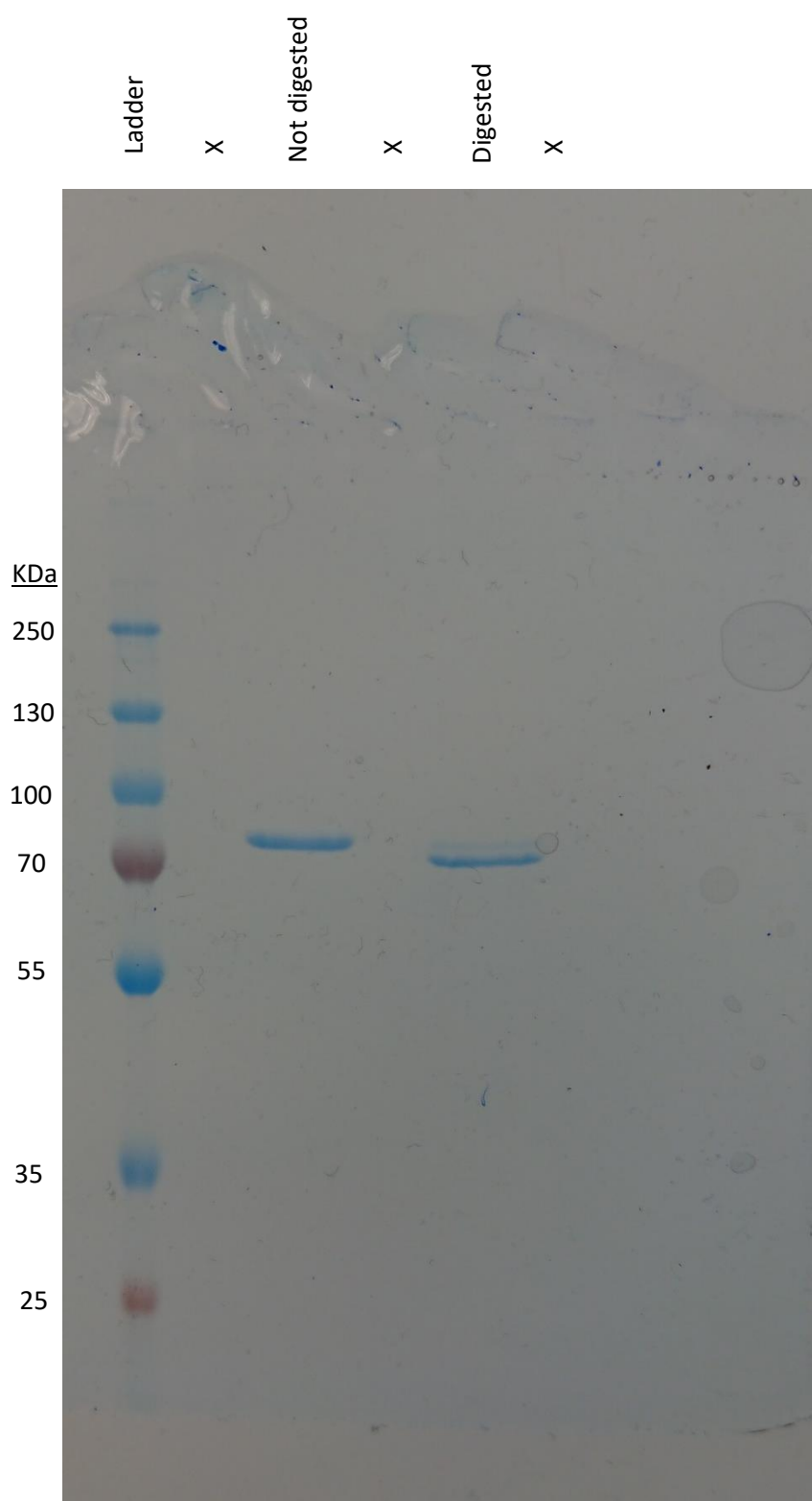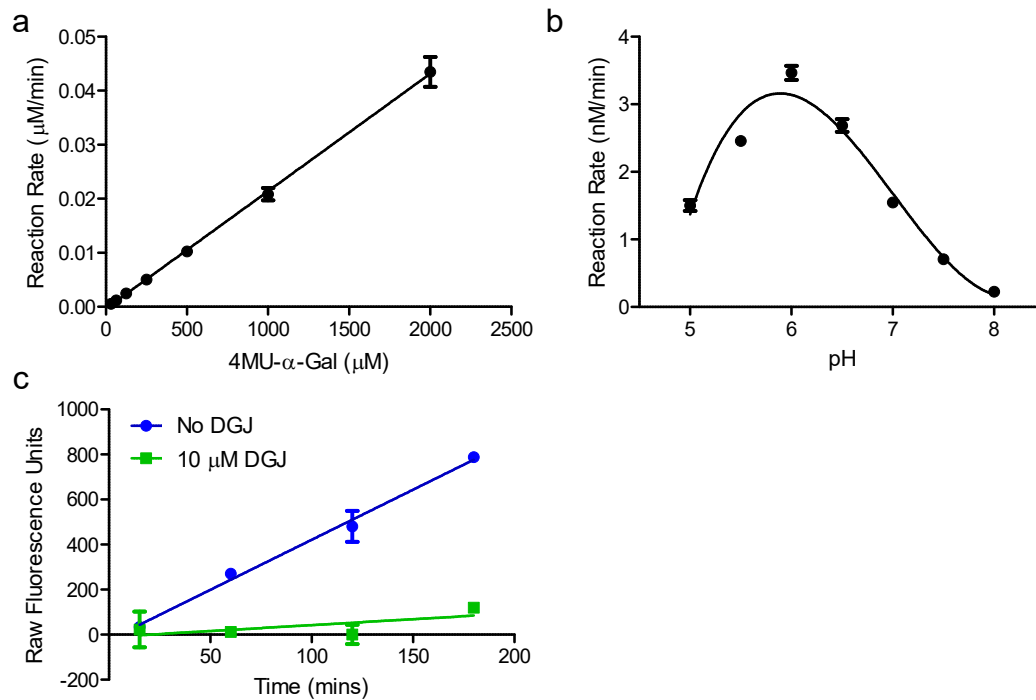
Figure S2. Analysis of MYORG kinetics against 4MU-α-D-galactopyranoside. a, Michaelis-Menten plot, k_{cat}/K_M was estimated from linear regression analysis. Three technical replicates ± standard error. **b,** pH activity profile of MYORG assayed in varying pH phosphate-citrate buffer. Three technical replicates ± standard error. **c,** Activity of MYORG in the presence and absence of 10 μM DGJ. Three technical replicates ± standard deviation. All raw data underlying graphs can be found in S1_Data.
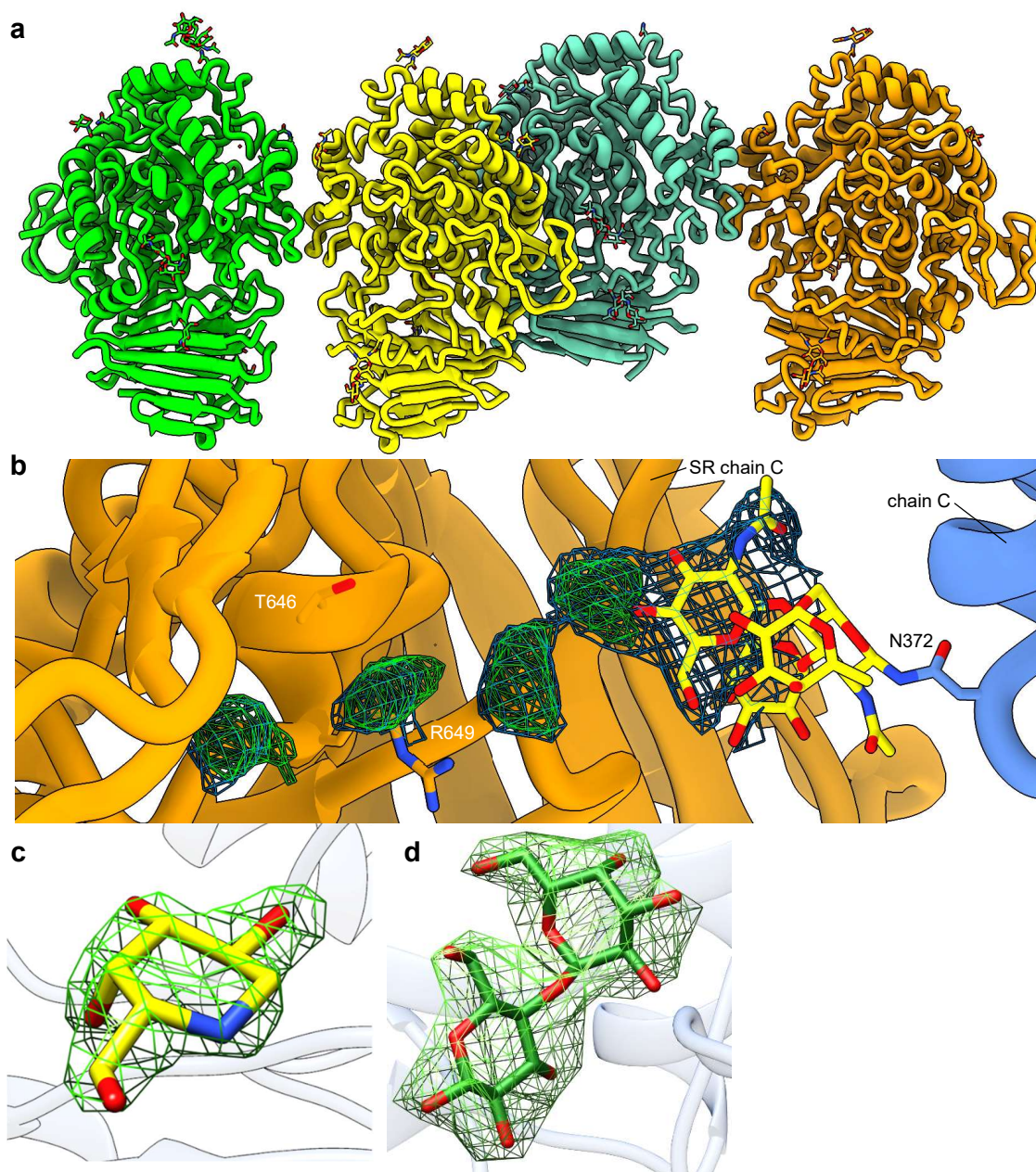
Figure S3. ASU contents and electron density figures. a, the asymmetric unit of MYORG. Four copies of MYORG depicted as cartoon ribbons comprise the ASU. Green and yellow chains form a dimer, as do the blue and orange chains. **b,** Transient crystal contacts likely provided by extension of the N-glycosylated N372 glycan. F_o-F_c (green mesh, 3 σ contour) and $2F_o$-F_c (blue mesh, 1 σ contour) electron density generated from the final model indicate the last modelled GlcNAc unit is extended further, however the electron density is too diffuse to accurately model further sugar units. SR, symmetry-related chain. **c,** Omit F_o-F_c electron density map for DGJ contoured to 3 σ. DGJ is superimposed onto the density to indicate placement. **d,** Omit F_o-F_c electron density for Gal-α1,4-Glc contoured to 3 σ. Gal-α1,4-Glc is superimposed onto the density to indicate placement.

```
                                                        1         10
HsMYORG     ..............................MLQNP.QEKSQAYPRRRRP
PsGal31A    ..........................................
EcYihQ      ..........................................
EcYicI      ............................MKISDGNWLIQP
FjDex31A    MKKSIFYCCVIFCIMVSQAYSQKKEQYLGNCTAYSVKGNKVVFSCANNSKI.......M.
Mm_aGlu-II  MA.....AIAAVAARRRRSWLSLVLAYLGVCLGITLAVDRSNFKTCDESSFCKRQRSIRP

            20        30        40
HsMYORG     GCYAYRQNPEAIA.......................AAAMYTFLP.............
PsGal31A    ..........................................
EcYihQ      ..........................................
EcYicI      GLNLIH...............PLQVFEVEQQDNEMVVYA....APRDVRERT
FjDex31A    ..........LQLCS.......GEVVKIWAS.....ADGNFVR.......NNESFAV
Mm_aGlu-II  GLSPYRALLDTLQLGPDALTVHLIHEVTKVLLVLELQGLQKNMTRIRIDELEPRRPRYRV

                                                50        60
HsMYORG     ...............DNFSPAKPK.....................P.SKDLKP.L.LGSAVLGLLL
PsGal31A    .........................MN......KFKK.LIQLF.C.LLFVA.LFYTS
EcYihQ      .....MDTPRPQLLDFQ...........FHQ.NNDS.F.T.LHFQQRLILTH
EcYicI      ...WQLDTPLFTLRFFSPQEGIVGV.....RIEHFQGA...LN.NGPHY.P.L.NILQDVKVTI
FjDex31A    IE........EDLGW....KGNVTVKEEPSTYEIFTEQLRIRV.N.KAP.FQ.L.LQIFDKYQKLL
Mm_aGlu-II  PDVLVADPPTARLSV....SGR...DDNSVELTVAEGPYKIIL.T.AQP.FR.L.DLLEDRSLLL

            70        80        90        100
HsMYORG     VLAAVVAWCY...YSVSLRKAERLRAELLDLKAGGFSIRNQKGE.............
PsGal31A    SHAQTANWTEIYPGV...WKATVGKPESYDLLKAAGAQPNKD.............ALSK
EcYihQ      SKDNPCLWIGSGIADIDMF.............RGNFSIKDK....LQEKIALTDAIVSQS
EcYicI      ENT....ERYAEFKS...............GNL.........SARVSK
FjDex31A    FSD....YAEKGFVN.................DNG.
Mm_aGlu-II  SVN......ARGLMAFEHQRAPRVPQESKDPAEGNGAQPEATPGDGDKPEETQEKAEKDE

            110       120                                  130
HsMYORG     .QVFRLAFRSGALDLD........................SCSRDGALLGCSLT
PsGal31A    TEKVSFPFANGGVS................LEVSGGKTYLRFPLQKEEQLYGFGLN
EcYihQ      PDGWLIHFSRGSDISATLNISADDQGRLLLELQNDNLNHNRIWLRLAAQPEDHIYGCGEQ
EcYicI      GEFWSLDFLRNGERITGSQVKN......NGYVQDTNNQRNYMFERLDLGVGETVYGLGER
FjDex31A    ..........KIRTNKVLRNDEQFFGLGEK
Mm_aGlu-II  PGAWEETFKTHSDS......K.........PY......GPTSVGLDFSLPGMEHVYGIPEH

            140       150       160       170       180
HsMYORG     ADG........LPLHFFIQTVRPKDTVMCYRVRWEEAAPGRAVEHAMFLGDAAAHWYGG
PsGal31A    FQT....VHQRGKILELHVD.....H...YGGK.............
EcYihQ      FSY....FDLRGKPFPLWTS......EQGVGRNK.............
EcYicI      FTA....LVRNGQTVETWNR....DGG....T.............
FjDex31A    SGN....LNRRGSAYKMWNS.....DQPCYGVN.............
Mm_aGlu-II  ADSLRLKVTEGGEPYRLYNL......DVFQYELN.............

            190       200       210       220       230       240
HsMYORG     AEMRTQHWPIRLD........GQQEPQPFVTSDVYSSDAAFGGILERYWLSSRAAAIKVN
PsGal31A    .D.SGRT........HAPTPFYVSS...N...GYG....VFINSARYIK....
EcYihQ      .Q.TYVTWQADCKENAGGDYYWTFFPQPTFVST...Q..KYY....CHVDNSCYMN....
EcYicI      .S.TEQA........YKNIPFYMTN...R...GYG....VLVNHPQCVS....
FjDex31A    .E..DPL........YKSIPFFMSS...Y..RYG....IFFDNTYKTE....
Mm_aGlu-II  .N.PMAL........YGSVPVLAHSFHR..DLG....IFWLNAAETW....

            250       260       270       280       290
HsMYORG     DSVPFHLGWNSTERSLRLQ...ARY.....HDTPYKPP.AGRAAAPELSYRVCVGSDVTS
PsGal31A    ....VWAGTGVRKDSENFPTPKDRNTDKTWSSRPYSDAVEILVPAEGVEVYVFGGPKPID
EcYihQ      ....FDFSAPEY.................HELALWEDK...AATLRFECADTYIS
EcYicI      ....FEVG.................SEKVSKVQFSVESEYLEYFVIDGPTPKA
FjDex31A    ....FKFG.................SESNDYYSFEAPAGQMVYYFMFGNDYKE
Mm_aGlu-II  ....VDISSNTAGKT.LFGKMLDYL...QGSGETPQTDIRWMSESGIIDVFLMLGPSVFD

            300       310       320       330       340       350
HsMYORG     IHKYMVRRYFNKPSRVPAPEAFRDPIWSTWALYGRAVDQDKVLRFAQQIRLHHFNSSHLE
PsGal31A    ....AVKRYNLLNGGGYLPPRWGLGFTQRVM...TRYTDKDVEKEVNDFKEKGYPLDFVG
EcYihQ      ....LLEKLTALLGRQPELPDWIYDGVTLGI...QG..GTEVCQKKLDTMRNAGVKVNGIW
EcYicI      ....VLDRYTRFTGRPALPPAWSFGLWLTTS.FTTNYDEATVNSFIDGMAERNLPLHVFH
FjDex31A    ....IIQNYIALTGKPIMPPKWALGFSQCRG...DYTREDQAREIAAEFRKRKIPCDIIY
Mm_aGlu-II  ....VFRQYASLTGTQALPPLFSLGYHQSRW...NYRDEADVLEVDQGFDDHNMPCDVIW

            360       370       380       390       400
HsMYORG     IDD.......MYTPAYGDFDFDEVKFPNASDMFRRLRDAGFRVTLWVHPFVNYNSS..R
PsGal31A    LEP....GWQS..KAYPGTFSWDKSRYPDPTSFVKKMKDQGIRLNLWINPYISPDAPF..
EcYihQ      AQDWSGIRMTSFGKRVMWNWKWNSENYPQLDSRIKQWNQEGVQFLAYINPYVASDKD..L
EcYicI      FDC....FW..MKAFQWCDFEWDPLTFPDPEGMIRRLKAKGLKICVWINPYIGQKSP..V
FjDex31A    QDI....GW..TEGLQ..DFDWRKNNYNNPKGMVKDLSDMGFKMIVSQDPVISQANQQQW
Mm_aGlu-II  LDI....EH..ADGKR..YFTWDPTRFPQPLNMLEHLASKRRKLVAIVDPHIKVDSGYRV
```

```
                    410         420         430         440         450
                    .           .           .           .           .
HsMYORG     FGEGVERELFVREPTGRLPALVRWWNGIGAVLDFTHPKARDWFQGHLRRLRSRYS..VAS
PsGal31A    YKEIK.......PYTGSHT.V...W..LGLVPDFTMAEARKPFFNQLLKDQIERG..VSG
EcYihQ      CEEAAQHGYLAKDASGGDYLVEF.GEFYGGVVDLTNPEAYAWFKEVIKKNMIELG..CGG
EcYicI      FKELQEKGYLLKRPDGSLWQ.WDKWQPGLAIYDFTNPDACKWYADKLKGLVAMG...VDC
FjDex31A    KEADALGHLVKDVRTGKSYDMPWPWGGNCGVVDFTKPEVADWWGSYQQKPLNDG...VRG
Mm_aGlu-II  HEELRNHGLYVKTRDGSDY.EGWCWPGSASYPDFTNPRMRAWWSNMFSFDNYEGSAPNLY

                460         470         480         490
                .           .           .           .
HsMYORG     FKFDAGEVSYLPRDFSTYRP.LPDPSVWSRRYTEMA....................LPF
PsGal31A    YKIDEVDG....YDYYLWPDAAKFPSGLSAEQMRQTYGLLVQRYSAELYK...QRNERTF
EcYihQ      WMADFGEYL.........PTDTYLHNGVSAEIMHNAWPALWAKCNYEAL.EETGKLGEIL
EcYicI      FKTDFGERI.........PTDVQWFDGSDPQKMHNHYAYIYNELVWNVL.KDTVGEEEAV
FjDex31A    FWTDMGEPAWSNEDAVDRLNMKHHLG..MHNEIHNVYGFTWDKVVTEQFY.KHNPNKRIF
Mm_aGlu-II  VWNDMNEPSVFNGPEVTMLKDAVHYGGWEHRDIHNIYGLYVHMATADGLIQRSGGIERPF
                 **

                500         510         520         530         540         550
                .           .           .           .           .           .
HsMYORG     FSLAEVRVGYQSQNISCFFRLVDRDSVW...GYDLGLRSLIPAVLTVSMLGYPFILPDMV
PsGal31A    GLVRASNGGGTS..FPYVIYN.DYYNH.........QDFITALINSGFAGV.LWTPEVR
EcYihQ      FFMRAGSTGSQK..YSTMMWAGDQNVDWSL...DDGLASVVPAALSLAMTGHGLHHSDIG
EcYicI      LFARSASVGAQK..FP.VHWGGDCY.....ANYESMAESLRGGLSIGLSGFGFWSHDIG
FjDex31A    QMTRAAYAGLQR..YT.FGWSGDSGNGSNVLDGWKQMANQIPVGLSAGMGLIPFWTCDIS
Mm_aGlu-II  VLSRAFFSGSQR..FG.AVWTGDNT......AEWDHLKISIPMCLSLALVGLSFCGADVG
                                   **

                560         570         580         590         600
                .           .           .           .           .
HsMYORG     GGNAVPQRTAGGDVPERELYIRWLEVAAFMPAMQFSI.......PPWRYDAEVVAIAQKF
PsGal31A    ..........ASKSGEEWLRRFQSNVFSPMAMINAW..ASGTKPWSYPEVEADVKKFA
EcYihQ      GYTTL.....FEMKRSKELLLRWCDFSAFTPMMRTHEG..NRPGDNWQFDGDAETIAHFA
EcYicI      GFENT.........APAHVYKRWCAFGLLSSHSRLHGS..KSYRVPWAYDDESCDVVRFF
FjDex31A    GYCGDI....KDYDAMAELYVRWLQFGVFTPLSRAHHE.GGNAVEPWKFGTEAENISRKS
Mm_aGlu-II  GFFKN.........PEPELLVRWYQMGAYQPFFRAHAHLDTGRREPWLLASQYQDAIRDA

                610         620         630         640
                .           .           .           .
HsMYORG     A..ALRASLVAPLLLELAGEVTDTGDPIVRPLWWIAP...................GDE
PsGal31A    L...LRM.QMMPYWYSAFARYHFEGMPPFRGMGLEEGFRQDAKVEKLNKVNLEENPYAEA
EcYihQ      RMTTVFT.TLKPYLKEAVALNAKSGLPVMRPLFLHYE....................DDA
EcYicI      T..QLKC.RMMPYLYREAARANARGTPMMRAMMMEFP....................DDP
FjDex31A    I..ELKY.KLFPYLYTYAREAHDTGLPIMRALLLEYP....................NDK
Mm_aGlu-II  L..FQRY.SLLPFWYTLFYQAHKEGFPVMRPLWVQYP....................EDM

                650         660         670         680         690         700
                .           .           .           .           .           .
HsMYORG     TAHRIDSQFLIGDTLLVAPVLEPGKQERDVYLPAGK..WRSYK.GELFDKTPVLLTDYPV
PsGal31A    ASKEIKDQYMAGDDLLVAPMFAG.EKSRKVVLPKGK..WYDFYTGEYAGDGEV.L.DVTP
EcYihQ      HTYTLKYQYLLGRDILVAPVHEEGRSDWTLYLPKGK..WVHAWTGEAFRGGEV...TVNA
EcYicI      ACDYLDRQYMLGDNVMVAPVFTE.AGDVQFYLPEGR..WTHLWHN.DELDGSRWH.KQQH
FjDex31A    ETFKLNGQFLVGKELLVAPVVEQGAVTKDVYLPEGE..WIDFNNCKTKYKGEQWI.TVDA
Mm_aGlu-II  STFSIEDQFMLGDALLIHPVSDAGAHGVQVYLPGQEEVWYDIQSY.QKHHGPQTL.YLPV

                710
                .
HsMYORG     DLDEIAYFTWAS................................................
PsGal31A    GLDKIPVYVRDGGIVPMMPALLNSPKSNQKVDLEIRY...YGNKPGEFKLYDDDGETFNY
EcYihQ      PIGKPPVFYRADSEWAALFASLKSI...................................
EcYicI      GFLSLPVYVRDNTLLALGNNDQRP.DYVWHEGTAFHL...........FNLQDGHEAVC
FjDex31A    PLNTIPVFVKKGSIIPQMPVMQYI.DEKKVYPVTFDIFPGNLNKETSFTFYEDDGESRDY
Mm_aGlu-II  TLSSIPVFQRGGTIVPRWMRVRRSSDCMKDDPITLFVALSPQG.TAQGELFLDDGHTFNY
```

Figure S4. Sequence alignment of MYORG against other CAZy GH31 family enzymes. Sequence numbered relative to MYORG. Orange double asterisk indicates nucleophile residue. Green double asterisk indicates acid/base residue. UniProt identifiers: Q6NSJ0 (*Hs*MYORG), A0A0F7R6D6 (*Ps*Gal31A), P32138 (*Ec*YihQ), P31434 (*Ec*YicI), A5FBI1 (*Fj*Dex31A) and Q8BHN3 (*Mm*α-Glu II).
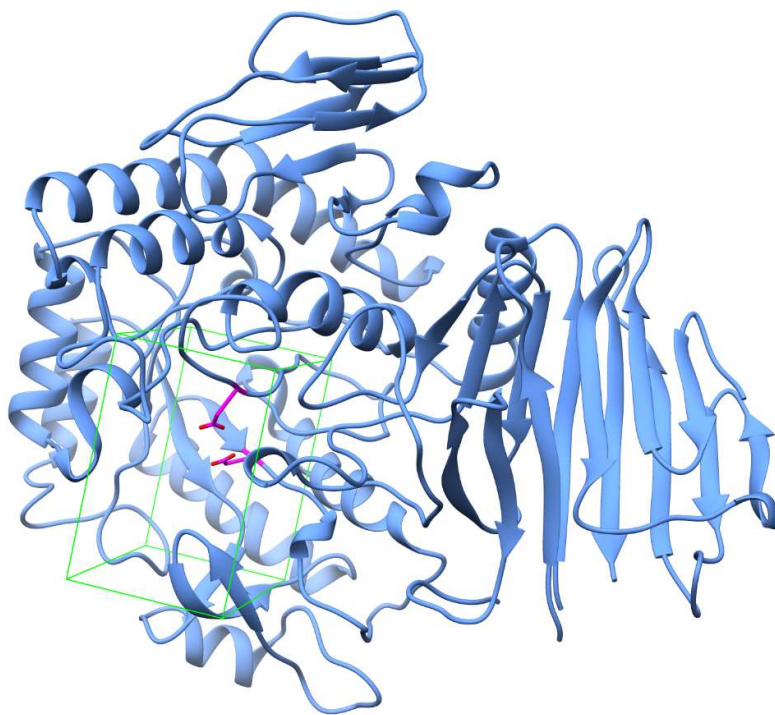
Figure S5. The region of MYORG used for docking simulations. Chain B of MYORG from the MYORG-Gal-α1,4-Glc complex was used for docking. Docking region enclosed in green square. Acid/base and nucleophile residue coloured in magenta.
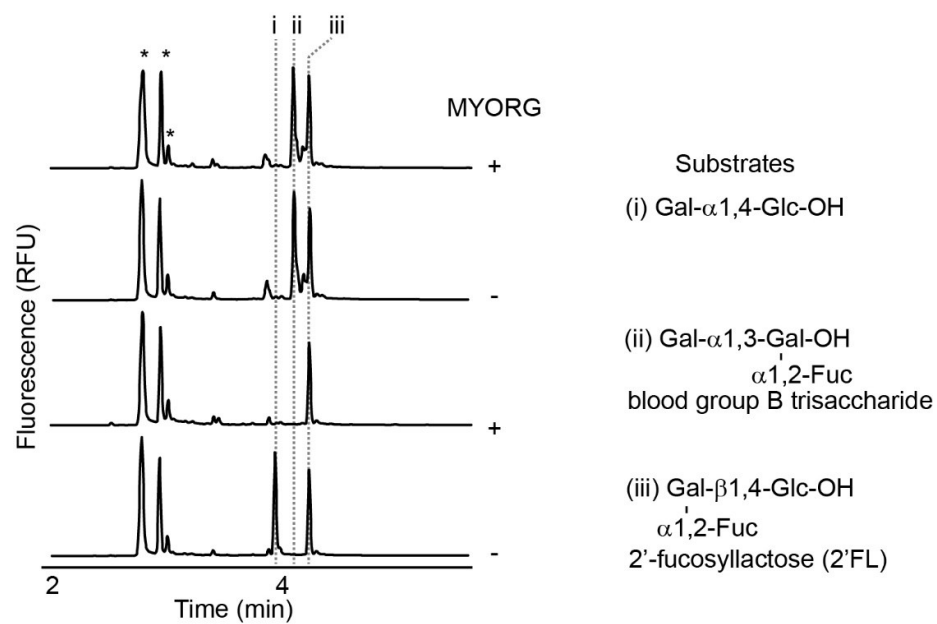
Figure S6. Representative CE-LIF electropherograms for candidate MYORG substrates. MYORG-active substrate (i) Gal-α1,4-Glc, MYORG-resistant substrate (ii) blood group B trisaccharide, and (iii) 2'-Fucosyllactose, which was included as an internal standard in all reactions. Peaks denoted with an asterisks (*) are due to excess fluorogenic reagents. Note that monosaccharides are lost during the desalting process prior to fluorescent labelling.

Table S1. Mutations identified in MYORG that cause PFBC and the associated structural consequences.

DNA change	Amino acid change	Location	Effect	Original Reference
c.103 A>G	M35V	N-terminal region	- Unknown	(1)
c.104 T>A	M35K	N-terminal region	- Unknown	(2)
c.191 G>A	G64E	Transmembrane helix	- Unknown	(3)
c.225 G>A	W75*	Transmembrane helix	- Severe truncation of protein.	(1)
c.285-310 del insert TTC	L95 fs	N-terminal domain	- Incorrect protein sequence from L95	(4)
c.337-348 dup	L113-R116 dup	N-terminal domain	- General disruption of protein fold.	(5)
c.338 T>G	L113R	N-terminal domain	- Disruption of hydrophobic core through steric clashes, caused by introduction of a large, charged sidechain.	(3)
c.348-349 insert CTGGCCTTCCGC	116-117 insert LAFR	N-terminal domain	- General disruption of protein fold.	(1)
	125-132 del CSRDGALL and insert	N-terminal domain	- Loss of stabilising di-sulphide bond. - General disruption of protein fold	(6)
c.428_442 del TGCACTTCTTCATCC	143_147 del LHFFI	N-terminal domain	- General disruption of protein fold	(7)
c.535-536 insert C	G179 fs	N-terminal domain	- Incorrect protein sequence from G179	(4)
c.607 C>T	Q203*	N-terminal domain	- Severe truncation of protein	(1)
c.679 C>G	R227G	N-terminal domain	- Loss of hydrogen bonding sidechain. R227 likely to aid in positioning of the loop carrying D213 (possible involved in binding polysaccharides at active site)	(8)
c.687 G>T	W229C	N-terminal domain	- Disruption of stabilising hydrophobic core.	(7)
c.695 C>T	S232L	N-terminal domain	- General disruption of structure through introduction of a larger sidechain causing steric clashes.	(1)
c.706_708 dup GCC	A236 dup	N-terminal domain	- Insertion of additional residue into β-sheet.	(3)
c.747G>C	W249C	N-terminal domain	- Disruption of stabilising hydrophobic core.	(3)

c.782-783 GC>TT	R261L	N-terminal domain	- Disruption of hydrogen bonding involved in the positioning of the loop carrying the likely active site residue D213. -Introduction of hydrophobic facing solvent	(1)
c.782 G>T	R261L			(8)
c.794 C>T	T265M	N-terminal domain	-Introduction of a bulky hydrophobic residue causing loop disruption.	(9)
c.830 del C	P277 fs	N-terminal domain	- Incorrect protein sequence from P277	(10)
c.850 T>C	C284R	N-terminal domain	-Breaks a disulphide bond and introduces a bulky charged residue causing fold disruption.	(2)
c.854_855 dup TG	G286W fs	N-terminal domain	- Loss of catalytic domain	(11)
c.856 G>A	G286S	N-terminal domain	-possible disruption of hydrophobic network affecting N-terminal domain fold.	(12)
c.893 G>C	R298P	Catalytic domain	- Disruption of α-helix	(8)
c.940 C>T	R314*	Catalytic domain	- Severe truncation of catalytic domain	(6)
c.1060_1062delGAC	354 del D	Catalytic domain	- D354 Is found in an active site loop, mutation would disrupt bonding of D353 to substrate and may also cause larger, global structural changes to MYORG through residue loss.	(13)
c.1078 del T	Y360 fs	Catalytic domain	- Loss of catalytic domain	(3)
c.1092-1097delCTTCGA	365-366 del FD	Catalytic domain	- F365 forms part of a hydrophobic core - General disruption of protein fold	(1)
c.1118 C>A	A373D	Catalytic domain	- Would cause steric clash leading to α-helix displacement. - May make N372 unavailable for glycosylation, possibly affecting protein production.	(3)
c.1233delC	F411L + fs	Insert	- Loss of catalytic domain.	(13)
c.1300 G>C	D434H	Insert	- Introduction of severe steric clashes.	(3)
c.1321 C>G	R441G	Catalytic domain	- Loss of stabilising salt bridge.	(1)

c.1328 G>A	W443*	Catalytic domain	- Loss of catalytic domain	(1)
c.1333 C>T	Q445*	Catalytic domain	- Loss of catalytic domain	(14)
c.1394 dup G	E466 fs	Catalytic domain	- Loss of catalytic domain	(3)
c.1427 C>A	T476N	Catalytic domain	- Likely to cause steric clashes.	(3)
c.1431 C>A	Y477*	Catalytic domain	- Loss of catalytic domain	(7)
c.1530 del G	N511T fs	Catalytic domain	- Loss of catalytic domain	(15)
c.1511 G>C	R504P	Catalytic domain	- Conserved residue associated with binding sugar substrates.	(8)
c.1538_1540 del CCT	513 del S	Catalytic domain	-Loss of stabilising hydrogen bond. - Would alter positioning of N511 possibly hindering glycosylation and protein processing. - Global structural issues likely from loss of amino acid.	(3)
c.1802_1804 del TGG	601 del V	Catalytic domain	- Loss of amino acid in α-helix affecting register/fold.	(8)
c.1831 C>T	R611W	Catalytic domain	- Disruption of important hydrogen bonding network. - Severe steric clashes introduced.	(3)
c.1865 T>C	L622P	Catalytic domain	- Disruption of α-helix	(3)
c.1967 T>C	I656T	Proximal β-sheet domain	- Disruption of stabilising hydrophobic core, anchoring proximal β-sheet domain to catalytic domain.	(16)
c.1979 T>A	L660Q	Proximal β-sheet domain	- Disruption of stabilising hydrophobic core, anchoring proximal β-sheet domain to catalytic domain.	(3)

Table S2. Data collection and refinement statistics for MYORG. Values in parenthesis are for highest-resolution shell. Each dataset was derived from a single crystal.

	Unliganded	DGJ complex	Gal-α1,4-Glc complex
Accession code	7QQF	7QQG	7QQH
Data Collection			
Spacegroup	*P*1	*P*1	*P*1
Cell dimensions			
a, b, c (Å)	74.1, 79.0, 180.1	73.1, 78.9, 176.2	73.3, 79.1, 178.0
α, β, γ (°)	88.1, 78.8, 62.7	80.8, 80.2, 62.6	80.9, 79.1, 62.7
Resolution (Å)	66.57-2.43	69.75-2.43	64.53-2.25
R_{meas}	0.093 (1.514)	0.103 (1.024)	0.103 (1.131)
$R_{p.i.m}$	0.066 (1.071)	0.073 (0.724)	0.073 (0.8)
I/σI	8.2 (1.0)	8.4 (1.4)	7.9 (1.0)
$CC_{1/2}$	0.983 (0.515)	0.995 (0.555)	0.99 (0.962)
Completeness	98.2 (96.9)	98.3 (97.4)	98.2 (96.7)
Multiplicity	2.2 (2.1)	3.5 (3.7)	3.1 (3.1)
Refinement			
Resolution	66.66-2.43	69.85-2.43	64.61-2.25
No. of reflections	125031	120841	153878
R_{work}/R_{free}	0.211/0.233	0.224/0.250	0.212/0.227
No. of atoms			
Protein	19414	18863	19824
Ligand	531	404	520
Water	319	233	486
B-factors			
Protein	62.83	61.05	54.39
Ligands	82.15	67.97	59.76
Waters	48.75	48.89	47.12
R.m.s. deviations			
Bond angles (°)	1.377	1.428	1.311
Bond lengths (Å)	0.0046	0.0060	0.0041

Table S3. Isothermal titration calorimetry results for MYORG. Values are the mean of two technical repeats ± standard deviations.

Compound	K_D (µM)	ΔH (kcal mol^{-1})	ΔG (kcal mol^{-1})	-TΔS (kcal mol^{-1})
DGJ	1.33 ± 0.45	-7.56 ± 0.21	-8.04 ± 0.21	-0.48 ± 0.85

References

1.	Yao XP, Cheng X, Wang C, Zhao M, Guo XX, Su HZ, et al. Biallelic Mutations in MYORG Cause Autosomal Recessive Primary Familial Brain Calcification. Neuron. 2018;98(6):1116-23.e5.

2.	Chen SY, Lin WC, Chang YY, Lin TK, Lan MY. Brain hypoperfusion and nigrostriatal dopaminergic dysfunction in primary familial brain calcification caused by novel MYORG variants: case report. BMC Neurol. 2020;20(1):329.

3.	Grangeon L, Wallon D, Charbonnier C, Quenez O, Richard AC, Rousseau S, et al. Biallelic MYORG mutation carriers exhibit primary brain calcification with a distinct phenotype. Brain. 2019;142(6):1573-86.

4.	Malaquias MJ, Martins RC, Oliveira J, Freixo JP, Magalhães M. MYORG gene disease-causing variants in a family with primary familial brain calcification presenting with stroke-like episodes. Clin Genet. 2020;98(5):517-9.

5.	Du J, Zhu X, Liu J, Tan Y. Paroxysmal Kinesigenic Dyskinesia Secondary to Brain Calcification with a Homozygous MYORG Mutation. Mov Disord. 2021.

6.	Taglia I, Kuipers DJS, Breedveld GJ, Mignarri A, Dotti MT, Federico A, et al. Primary familial brain calcification caused by MYORG mutations in an Italian family. Parkinsonism Relat Disord. 2019;67:24-6.

7.	Chen Y, Fu F, Chen S, Cen Z, Tang H, Huang J, et al. Evaluation of MYORG mutations as a novel cause of primary familial brain calcification. Mov Disord. 2019;34(2):291-7.

8.	Chen Y, Cen Z, Chen X, Wang H, Chen S, Yang D, et al. MYORG Mutation Heterozygosity Is Associated With Brain Calcification. Mov Disord. 2020;35(4):679-86.

9.	Kume K, Takata T, Morino H, Matsuda Y, Ohsawa R, Tada Y, et al. The first Japanese case of primary familial brain calcification caused by an MYORG variant. J Hum Genet. 2020;65(10):917-20.

10.	Gao L, Chen J, Dong H, Li X. A novel mutation in MYORG leads to primary familial brain calcification and cerebral infarction. Int J Neurosci. 2021:1-5.

11.	Ferreira LD, de Oliveira JRM. New homozygous indel in MYORG linked to brain calcification, thyroidopathy and neuropathy. Brain. 2019;142(9):e51.

12.	Tekin Orgun L, Besen Ş, Sangün Ö, Bisgin A, Alkan Ö, Erol İ. First pediatric case with primary familial brain calcification due to a novel variant on the MYORG gene and review of the literature. Brain Dev. 2021;43(7):789-97.

13.	Arkadir D, Lossos A, Rahat D, Abu Snineh M, Schueler-Furman O, Nitschke S, et al. MYORG is associated with recessive primary familial brain calcification. Ann Clin Transl Neurol. 2019;6(1):106-13.

14.	Peng Y, Wang P, Chen Z, Jiang H. A novel mutation in MYORG causes primary familial brain calcification with central neuropathic pain. Clin Genet. 2019;95(3):433-5.

15.	Ramos EM, Roca A, Chumchim N, Dokuru DR, Van Berlo V, De Michele G, et al. Primary familial brain calcification caused by a novel homozygous MYORG mutation in a consanguineous Italian family. Neurogenetics. 2019;20(2):99-102.

16.	Forouhideh Y, Müller K, Ruf W, Assi M, Seker T, Tunca C, et al. A biallelic mutation links MYORG to autosomal-recessive primary familial brain calcification. Brain. 2019;142(2):e4.